



**HAL**  
open science

## Equations of state in the Fe-FeSi system at high pressures and temperatures

Rebecca A. Fischer, Andrew J. Campbell, Razvan Caracas, Daniel M. Reaman, Dion L. Heinz, Przemyslaw Dera, Vitali B. Prakapenka

► **To cite this version:**

Rebecca A. Fischer, Andrew J. Campbell, Razvan Caracas, Daniel M. Reaman, Dion L. Heinz, et al.. Equations of state in the Fe-FeSi system at high pressures and temperatures. *Journal of Geophysical Research: Solid Earth*, 2014, 119 (4), pp.2810-2827. 10.1002/2013JB010898 . hal-02350693

**HAL Id: hal-02350693**

**<https://univ-lyon1.hal.science/hal-02350693>**

Submitted on 21 May 2021

**HAL** is a multi-disciplinary open access archive for the deposit and dissemination of scientific research documents, whether they are published or not. The documents may come from teaching and research institutions in France or abroad, or from public or private research centers.

L'archive ouverte pluridisciplinaire **HAL**, est destinée au dépôt et à la diffusion de documents scientifiques de niveau recherche, publiés ou non, émanant des établissements d'enseignement et de recherche français ou étrangers, des laboratoires publics ou privés.

## RESEARCH ARTICLE

10.1002/2013JB010898

## Key Points:

- We determined equations of state of Fe–9Si and FeSi to 200 and 145 GPa
- Outer core contains up to ~11–12 wt % Si based on density and sound speed
- Inner core contains up to ~6–8 wt % Si based on density and sound speed

## Supporting Information:

- Readme
- Table S1
- Table S2
- Table S3
- Table S4
- Table S5
- Table S6
- Table S7
- Text S1
- Figure S1
- Figure S2
- Figure S3
- Figure S4

## Correspondence to:

R. A. Fischer,  
rfischer@uchicago.edu

## Citation:

Fischer, R. A., A. J. Campbell, R. Caracas, D. M. Reaman, D. L. Heinz, P. Dera, and V. B. Prakapenka (2014), Equations of state in the Fe–FeSi system at high pressures and temperatures, *J. Geophys. Res. Solid Earth*, 119, 2810–2827, doi:10.1002/2013JB010898.

Received 14 DEC 2013

Accepted 9 MAR 2014

Accepted article online 15 MAR 2014

Published online 15 APR 2014

## Equations of state in the Fe–FeSi system at high pressures and temperatures

Rebecca A. Fischer<sup>1</sup>, Andrew J. Campbell<sup>1</sup>, Razvan Caracas<sup>2</sup>, Daniel M. Reaman<sup>1</sup>, Dion L. Heinz<sup>1</sup>, Przemyslaw Dera<sup>3,4</sup>, and Vitali B. Prakapenka<sup>3</sup>

<sup>1</sup>Department of the Geophysical Sciences, University of Chicago, Chicago, Illinois, USA, <sup>2</sup>Centre National de la Recherche Scientifique, Laboratoire de Sciences de la Terre, Ecole Normale Supérieure de Lyon, University of Claude Bernard–Lyon, Lyon, France, <sup>3</sup>GeoSoilEnviroCARS, University of Chicago, Chicago, Illinois, USA, <sup>4</sup>Now at Hawaii Institute of Geophysics and Planetology, School of Ocean and Earth Science and Technology, University of Hawai'i at Manoa, Honolulu, Hawaii, USA

**Abstract** Earth's core is an iron-rich alloy containing several weight percent of light element(s), possibly including silicon. Therefore, the high pressure-temperature equations of state of iron-silicon alloys can provide understanding of the properties of Earth's core. We performed X-ray diffraction experiments using laser-heated diamond anvil cells to achieve simultaneous high pressures and temperatures, up to ~200 GPa for Fe–9 wt % Si alloy and ~145 GPa for stoichiometric FeSi. We determined equations of state of the D0<sub>3</sub>, hcp + B2, and hcp phases of Fe–9Si, and the B20 and B2 phases of FeSi. We also calculated equations of state of Fe, Fe<sub>11</sub>Si, Fe<sub>5</sub>Si, Fe<sub>3</sub>Si, and FeSi using ab initio methods, finding that iron and silicon atoms have similar volumes at high pressures. By comparing our experimentally determined equations of state to the observed core density deficit, we find that the maximum amount of silicon in the outer core is ~11 wt %, while the maximum amount in the inner core is 6–8 wt %, for a purely Fe–Si–Ni core. Bulk sound speeds predicted from our equations of state also match those of the inner and outer core for similar ranges of compositions. We find a compositional contrast between the inner and outer core of 3.5–5.6 wt % silicon, depending on the seismological model used. Theoretical and experimental equations of state agree at high pressures. We find a good match to the observed density, density profile, and sound speed of the Earth's core, suggesting that silicon is a viable candidate for the dominant light element.

## 1. Introduction

The Earth's core is primarily an iron-nickel alloy, but it must also contain several weight percent of one or more elements that are lighter than iron in order to match the observed core density [Birch, 1952]. Many elements have been proposed to comprise this light element component, with the most prominent candidates including silicon, oxygen, sulfur, carbon, and hydrogen [e.g., Allègre *et al.*, 1995; McDonough, 2003]. Silicon has been frequently proposed as the dominant light element in the Earth's core, because it is abundant in the silicate Earth, it is found in the metal of some chondritic meteorites, a core reservoir of silicon is permitted by comparisons of the Mg/Si and Fe/Si ratios of the Earth and chondrites, and silicon is known to partition into iron metal under reducing conditions [Allègre *et al.*, 1995; McDonough, 2003]. Experiments have shown that this partitioning behavior continues to very high pressures [e.g., Knittle and Jeanloz, 1991; Ozawa *et al.*, 2008, 2009; Siebert *et al.*, 2012; Takafuji *et al.*, 2005]. Silicon in the core may also be able to explain the nonchondritic <sup>30</sup>Si/<sup>28</sup>Si ratios in terrestrial rocks [Fitoussi *et al.*, 2009; Georg *et al.*, 2007; Shahar *et al.*, 2009]. Previous studies have estimated the maximum silicon content of the core using many methods, producing numbers ranging from less than 4 wt % [Antonangeli *et al.*, 2010] to ~5–7 wt % [Allègre *et al.*, 1995; Brosh *et al.*, 2009; Javoy *et al.*, 2010; McDonough, 2003; Shahar *et al.*, 2009; Siebert *et al.*, 2012; Wade and Wood, 2005] to 8–13 wt % [Fischer *et al.*, 2012; Lin *et al.*, 2003; Mao *et al.*, 2012; Ricolleau *et al.*, 2011; Rubie *et al.*, 2011; Sata *et al.*, 2010] to up to 20 wt % [Ahrens, 1982; Balchan and Cowan, 1966; Ringwood, 1959].

The light element composition of the core has implications for planetary formation, core segregation, core dynamics, metal-silicate reactions, thermal evolution of the core, and generation of the geodynamo [e.g., Allègre *et al.*, 1995; Chabot *et al.*, 2011; Deguen, 2012; Javoy *et al.*, 2010; Righter, 2011; Stevenson, 1981]. Equations of state of Fe–Si alloys can be used to constrain the maximum silicon content of the Earth's core and evaluate the likelihood of silicon as a core component by comparison to the core density, compressibility, and sound velocities in the Preliminary Reference Earth Model (PREM) [Dziewonski and Anderson, 1981]. In this

study, we report on the high pressure-temperature ( $P$ - $T$ ) equations of state of Fe–9 wt % Si (hereafter Fe–9Si) and stoichiometric FeSi, combining our results with the equations of state of pure iron [Dewaele *et al.*, 2006] and Fe–16Si [Fischer *et al.*, 2012] to evaluate silicon as a core component and identify the effects of composition on the equations of state of iron-silicon alloys.

Alloys with compositions near Fe–9Si have been the subjects of several previous studies. Fischer *et al.* [2013] reported on the subsolidus phase diagram and melting curve of this alloy to 200 GPa. At high pressures, it has the hexagonal close packed (hcp) crystal structure at low temperatures. With increasing temperature, it converts to a mixture of the hcp and B2 (CsCl-type) structures, then to a mixture of face-centered cubic (fcc) and B2 structures. Morard *et al.* [2011] measured two melting points of Fe–5Ni–10Si at high pressures. Lin *et al.* [2002, 2009] investigated the subsolidus phase diagram of Fe–7.9Si, while Kuwayama *et al.* [2009] studied the phase diagram of Fe–9.9Si. Lin *et al.* [2003] reported a room temperature equation of state of Fe–7.9Si and Hirao *et al.* [2004] of Fe–8.7Si. Zhang and Guyot [1999a, 1999b] studied the phase diagram and equation of state of Fe–8.9Si in a large volume press to 9 GPa and 773 K. In this study, we seek to construct a thermal equation of state of Fe–9Si to pressures and temperatures of the Earth's core.

Stoichiometric FeSi has also been previously studied. Fischer *et al.* [2013] report on its high  $P$ - $T$  phase diagram to 145 GPa. It has the B20 (FeSi-type) structure at lower pressures, the B2 structure at high pressures, and a wide two-phase region in between. Knittle and Williams [1995] and Lin *et al.* [2003] measured the 300 K equation of state of B20 FeSi, while Guyot *et al.* [1997] determined its thermal equation of state in a large volume press. The B2 structure was predicted theoretically by Vočadlo *et al.* [1999] and confirmed experimentally by Dobson *et al.* [2002]. The equation of state and phase diagram of FeSi was also studied theoretically by Caracas and Wentzcovitch [2004]. Dobson *et al.* [2003], Sata *et al.* [2010], and Ono *et al.* [2007] report room temperature equations of state for B2 FeSi. Melting of FeSi has been investigated by Fischer *et al.* [2013], Lord *et al.* [2010], and Santamaría-Pérez and Boehler [2008]. Recently, Ono [2013] calculated a thermal equation of state of B2 FeSi using ab initio methods, constrained by experimental data at 300 K. However, there exists no experimentally determined thermal equation of state of B2 FeSi, which will be a focus of this study.

## 2. Methods

The methods used in this study are similar to those of Fischer *et al.* [2013]. Our sample materials were Fe–9Si (Goodfellow Corporation) and stoichiometric FeSi (Alfa Aesar). Measurements of composition and structure of our materials were first made at atmospheric pressure by electron microprobe and X-ray diffraction [Miller, 2009]. The material was then pressed in a diamond anvil cell to produce a foil  $\sim 3 \mu\text{m}$  thick and loaded into a rhenium gasket between layers of KBr, each  $\sim 10 \mu\text{m}$  thick. The sample assembly was oven dried at  $\sim 90^\circ\text{C}$  for approximately 1 h after cell loading but before the cell was closed to remove any moisture.

Laser-heating angle-dispersive X-ray diffraction experiments were performed at beamline 13-ID-D (GeoSoilEnviro Center for Advanced Radiation Sources (GSECARS)) of the Advanced Photon Source (APS) at Argonne National Laboratory [Prakapenka *et al.*, 2008; Shen *et al.*, 2005]. The incident X-ray beam was monochromatic ( $\lambda = 0.3344 \text{ \AA}$ ) and measured  $\sim 4 \mu\text{m} \times 4 \mu\text{m}$ . X-ray-induced fluorescence of the KBr pressure medium was used to coalign the optical axes of the laser heating and temperature measurement system with the X-ray beam, which were still aligned following heating. The sample was laser heated from each side by 1064 nm Yb fiber lasers with flat top intensity profiles, with the laser power on each side being independently adjustable to minimize axial temperature gradients [Prakapenka *et al.*, 2008]. Diffraction patterns were collected on heating and cooling. Temperatures were determined by spectroradiometry using the graybody approximation, and one temperature measurement was made simultaneously with each diffraction pattern. Laser-heated spots were  $\sim 20 \mu\text{m}$  in diameter across the flat top region, much larger than the X-ray beam to minimize radial temperature gradients. Temperatures were measured from an area comparable to the size of the region probed by the X-rays. The sample temperature was an average of upstream and downstream temperatures, corrected downward by  $\sim 3\%$  to account for a small axial temperature gradient through the sample [Campbell *et al.*, 2007, 2009]. Reported temperature uncertainties include an analytical uncertainty of 100 K [Shen *et al.*, 2001], the difference between upstream and downstream temperatures, and uncertainty from the thickness correction [Campbell *et al.*, 2007, 2009]. Temperature measurements in the diamond cell were benchmarked by analyzing a sample of iron in MgO to check the location of the hcp-fcc transition in iron [Fischer *et al.*, 2011, 2012].

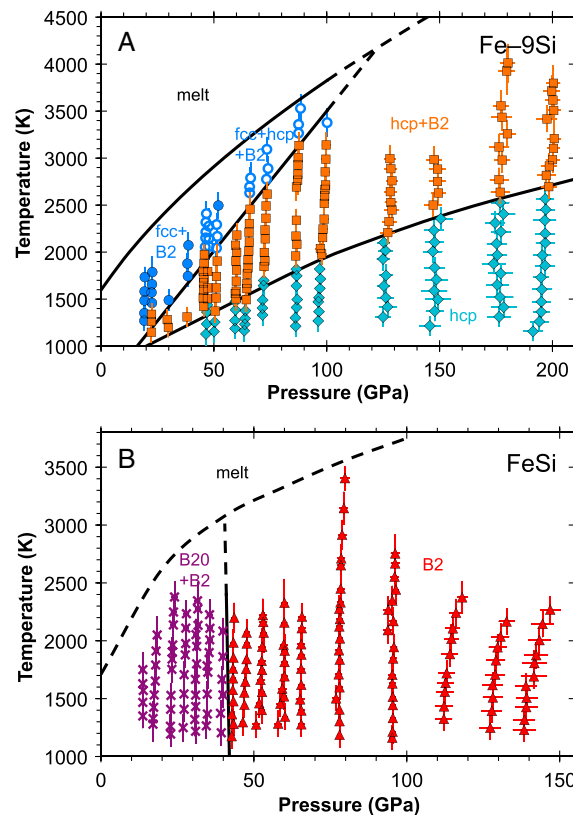


**Figure 1.** Pressure-temperature phase diagrams illustrating the range of high-temperature data coverage, after Fischer et al. [2013]. Data are listed in Tables S1 and S2 in the supporting information. (a) *P-T* data of Fe–9Si. Teal diamonds: hcp structure. Orange squares: hcp + B2 mixture. Solid blue circles: fcc + B2 mixture. Open blue circles: metastable fcc + hcp + B2 mixture. Melting curve is from Fischer et al. [2013]. (b) *P-T* coverage of stoichiometric FeSi. Purple cross symbols: B20 + B2 mixture. Red triangles: B2 structure. Melting curve is from Lord et al. [2010].

Two-dimensional diffraction images were integrated using the Fit2D program [Hammersley et al., 1996], then peak fitting was performed using PeakFit (Systat Software). Overlapping peaks were deconvolved in the peak fitting process whenever possible and were not used in the equation of state fits if they could not be deconvolved. Pressures were determined from the volume of B2 KBr [Fischer et al., 2012], with the lattice parameter and its uncertainty determined as the average and standard error from multiple *d*-spacings. Uncertainties in pressure were propagated from uncertainties in temperature and lattice parameter. The KBr temperature during laser heating was less than the measured temperature, due to axial thermal gradients through the insulator, so it was corrected downward [Campbell et al., 2009].

Samples for room temperature compression were loaded in neon using the Consortium for Materials Properties Research in Earth Sciences (COMPRES)/GSECARS gas-loading system at the APS [Rivers et al., 2008]. Pressure standards were KBr and ruby [Fischer et al., 2012; Mao et al., 1986]. Room temperature compression of FeSi was performed at APS, while compression of Fe–9Si was done at beamline 12.2.2 of the Advanced Light Source (ALS), Lawrence Berkeley National Laboratory [Kunz et al., 2005]. At the ALS we used a monochromatic incident beam ( $\lambda = 0.41323 \text{ \AA}$ ) measuring  $30 \mu\text{m} \times 30 \mu\text{m}$ .

In parallel to experiments, we also performed first-principles calculations based on the planar-augmented wave function formalism [Blöchl, 1994] of the density-functional theory in the ABINIT implementation [Gonze et al., 2002, 2009]. We used the generalized-gradient approximation for the exchange-correlation functional [Perdew et al., 1996], with parameters similar to the ones in our previous study [Fischer et al., 2012]. We built the structures starting with hcp iron and replacing Fe by Si in the desired amounts in various supercells. We performed the substitutions in several patterns to consider several Si concentrations in the hcp iron and to mimic the effect of order-disorder relations. As both end-member hcp iron and B2 FeSi are nonmagnetic, our simulations are non-spin polarized. All structures were relaxed at static conditions ( $T = 0 \text{ K}$ ).

### 3. Results

#### 3.1. Fe–9Si Results

The pressure-volume-temperature (*P-V-T*) data from the synchrotron X-ray diffraction experiments on Fe–9Si are listed in Table S1 in the supporting information. Figure 1a illustrates our high-temperature data coverage in *P-T* space. Figure 2 shows our data in *P-V* space. These data extend to pressures of over 200 GPa and temperatures up to ~4000 K. In all experiments, pressure was determined from the lattice parameter of B2 KBr, which was calculated from the *d*-spacings of four to 13 of the following *hkl* peaks: 100, 110, 111, 200, 210, 211, 220, 221 + 300, 310, 311, 222, 320, and 321.

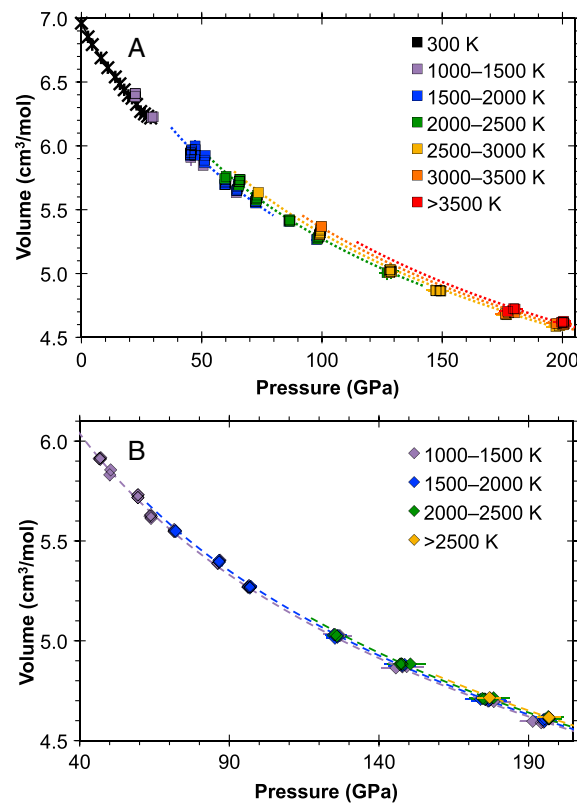


**Figure 2.** Equations of state of Fe-9Si. (a) Equations of state of the  $D0_3$  structure and the hcp + B2 mixture. Cross symbols:  $D0_3$  volumes at 300 K. Squares: average volumes of B2 and hcp structures. Symbols are measured volumes, while lines are isotherms calculated from the fitted equations of state. Solid line:  $D0_3$ . Dotted lines: hcp + B2. All data and isotherms are color coded according to the legend, with isotherms calculated for the midpoint of the indicated temperature range. Isotherms are truncated at phase boundaries and where unconstrained by data. The  $D0_3$  isotherm is likely shown outside its stability field due to slow kinetics at 300 K. (b) Equation of state of the hcp structure, where it does not coexist with any other phases. Diamonds: hcp volumes. Dashed lines: calculated hcp isotherms.

The Fe-9Si alloy has the  $D0_3$  ( $BiF_3$ -type; space group  $Fm\bar{3}m$ ) crystal structure at ambient conditions [Massalski, 1986] and under room temperature compression to 29 GPa [Fischer *et al.*, 2013]. This may not accurately represent the stability field of this structure due to slow kinetics of phase transitions at 300 K. The  $D0_3$  structure is an ordered version of the B2 (CsCl-type; space group  $Pm\bar{3}m$ ) structure, which is an ordered version of the body-centered cubic (bcc) structure. The lattice parameter of  $D0_3$  Fe-9Si was determined from three to seven of the following  $hkl$  peaks: 111, 200, 220, 311, 222, 400, and 331.

The high  $P$ - $T$  phase diagram of Fe-9Si was reported in Fischer *et al.* [2013] and can be seen in Figure 1a. At high pressures, the Fe-9Si alloy has the hcp crystal structure. With increasing temperature, it converts to an hcp + B2 mixture, then to an fcc + B2 mixture. At high temperatures the hcp structure sometimes persists, likely reflecting slow kinetics of this transition [Fischer *et al.*, 2013]. Examples of X-ray diffraction patterns on Fe-9Si at high pressures and temperatures can be seen in Figure 3. The lattice parameters and  $c/a$  ratio of the hcp structure were determined from up to nine of the following  $hkl$  peaks: 100, 002, 101, 102, 110, 103, 200, 112, 201, 004, and 202. The B2 lattice parameter was measured using up to seven of the following peaks: 100, 110, 111, 200, 210, 211, 220, and 221 + 300. The fcc lattice parameter was determined from up to four of the following peaks: 111, 200, 220, 311, 222, and 400.

### 3.2. FeSi Results

The  $P$ - $V$ - $T$  data from the synchrotron X-ray diffraction experiments on stoichiometric FeSi are listed in Table S2 in the supporting information, and our high-temperature data coverage in  $P$ - $T$  space can be seen in Figure 1b. We report all volumes of FeSi in units of cubic centimeters per mole of atoms, instead of cubic centimeters per mole of formula units, to simplify comparison to other Fe-Si alloys. Figure 4 shows our data in  $P$ - $V$  space. They extend to pressures of  $\sim 145$  GPa and temperatures of up to 3400 K.

FeSi has the B20 (FeSi-type; space group  $P2_13$ ) crystal structure at ambient conditions and under room temperature compression to 36 GPa [Fischer *et al.*, 2013]. Again, this may not accurately represent the stability field of this structure due to slow kinetics of phase transitions at 300 K. The B20 structure may be thought of as a distortion of the B1 (NaCl-type) crystal structure. The lattice parameter of the B20 structure was determined from the  $d$ -spacings of up to 10 of the following  $hkl$  peaks: 110, 111, 200, 210, 211, 220, 221 + 300, 310, 311, 222, 320, 321, 400, 331, 420, 421, and 332. FeSi converts from the B20 structure to a B20 + B2 mixture with increasing pressure (at or below 14 GPa at high temperatures), then converts fully to the B2 structure by  $\sim 42$  GPa [Fischer *et al.*, 2013] (Figure 1b). This result is different from some, but not all, earlier ex situ data [Dobson *et al.*, 2002; Lord *et al.*, 2010], as discussed in Fischer *et al.* [2013]. The B2 lattice parameter was

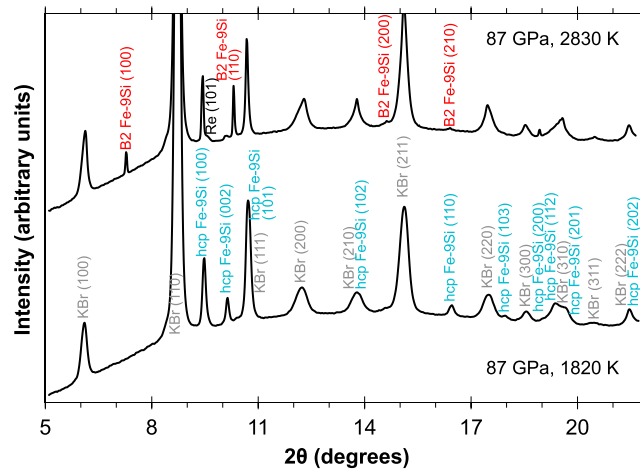


**Figure 3.** X-ray diffraction patterns of Fe-9Si, collected on heating at ~87 GPa. (bottom) Pattern collected at 1820 K, with peaks from B2 KBr and hcp Fe-9Si. (top) Pattern collected during the same heating cycle at 2830 K. Peaks correspond to B2 KBr, hcp Fe-9Si, and B2 Fe-9Si, with one faint reflection from the rhenium gasket. KBr and hcp peaks are the same as those in the lower pattern and are unlabeled for clarity. The presence of the B2 Fe-9Si 100 peak indicates that the alloy has the B2 structure, not the bcc structure.

pure iron, Fe<sub>11</sub>Si (Fe-4Si), Fe<sub>5</sub>Si (Fe-9Si), Fe<sub>3</sub>Si (Fe-14Si), and FeSi. Several ordering patterns have been calculated for Fe<sub>5</sub>Si and Fe<sub>3</sub>Si. The data span up to pressures of 400 GPa in 20 GPa increments. These *P-V* data can be found in Table S3 in the supporting information.

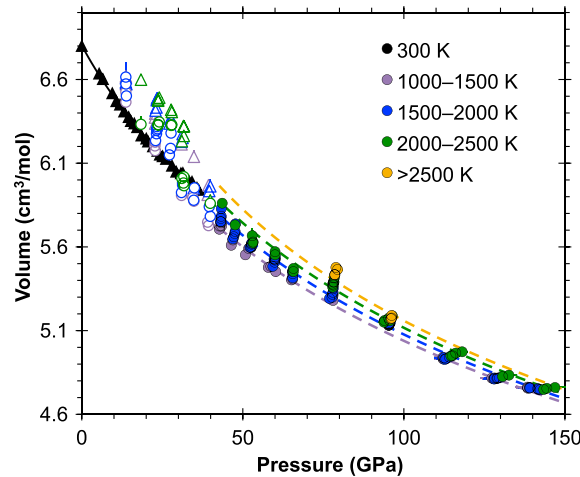


**Figure 4.** Equations of state of stoichiometric FeSi. Triangles: B20 structure. Circles: B2 structure. Symbols are measured volumes, while lines are isotherms calculated from the fitted equations of state. Solid line: B20. Dashed lines: B2. All data and isotherms are color coded according to the legend, with isotherms calculated for the midpoint of the indicated temperature range. B2 isotherms begin at phase boundary; the B20 isotherm is likely shown outside its stability field due to slow kinetics at 300 K. Closed symbols indicate data used in fitting, where only one phase is stable; open symbols indicate data where both phases are stable. In the mixed phase region from 10 to 40 GPa at high temperature, volumes of individual phases are shown. The compositions of these phases are uncertain, which may cause deviation from the equations of state that were fitted to the single-phase data.

calculated from up to seven of the following peaks: 100, 110, 111, 200, 210, 211, 220, 221 + 300, and 310. Figure 5 shows an X-ray diffraction pattern of B2 FeSi at high pressures and temperatures. The B2 structure of FeSi is stable to at least 145 GPa at high temperatures [Fischer *et al.*, 2013] (Figure 1b).

### 3.3. Computational Results

Pressures and volumes have been calculated in the hcp structure at 0 K for several silicon concentrations. We built various supercells: 1 × 1 × 1, 1 × 1 × 2, 1 × 1 × 3, 1 × 2 × 2, 2 × 2 × 2, 1 × 2 × 3, and we replaced one or more Fe atoms with correspondingly one or more Si atoms in different replacement patterns. In this way we were able to simulate the effects of ordering on the equations of state and specific volumes. We obtained data for the following stoichiometries:

## 4. Experimental Equations of State

### 4.1. Equations of State of Fe-9Si

We fit our experimental *P-V* data set for D0<sub>3</sub> Fe-9Si at room temperature to a third-order Birch-Murnaghan equation of state

$$P(V) = 3K_0 f(1 + 2f)^{5/2} \left[ 1 + \frac{3}{2} f(K'_0 - 4) \right] \quad (1)$$

with 1 bar isothermal bulk modulus  $K_0$ , its pressure derivative  $K'_0$ , and Eulerian strain  $f = [(V/V_0)^{-2/3} - 1]/2$  [Birch, 1952]. Table 1 shows the equation of state parameters we found for D0<sub>3</sub> Fe-9Si alloy. We fit  $K_0$  and  $K'_0$ , fixing the zero-pressure volume to the value we measured experimentally. A 300 K isotherm calculated from our equation of state for D0<sub>3</sub> Fe-9Si can be seen in Figure 2a. Figure S1a in the supporting information illustrates the pressure residuals in our equation of state fit for D0<sub>3</sub> Fe-9Si, which range from -1.1 to 0.5 GPa.

Lin *et al.* [2003] and Hirao *et al.* [2004] determined room temperature equations of state of bcc-like Fe-7.9Si and Fe-8.7Si, respectively. The equation of state parameters they found are listed in Table 1. They report the structure of their alloys as bcc, but it was likely the D0<sub>3</sub> structure, based on the 1 bar phase diagram

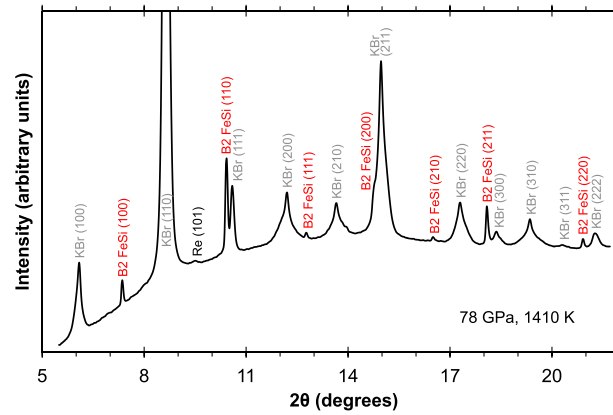


**Figure 5.** X-ray diffraction pattern of FeSi, collected at 1410 K and 78 GPa on cooling. Peaks correspond to the KBr pressure medium and B2 FeSi, with one faint reflection from the rhenium gasket.

[Massalski, 1986] and the difficulty in identifying the ordered D0<sub>3</sub> structure in high-pressure diffraction patterns [Fischer et al., 2013]. Hirao et al. [2004] report that the strongly nonhydrostatic conditions in their experiments likely caused an overestimate of K<sub>0</sub>. Zhang and Guyot [1999a] report a thermal equation of state of bcc-like Fe–9Si. However, based on the 1 bar phase diagram in the Fe–Si system from Massalski [1986], their high-temperature data likely span one or more ordering transitions, with their data set probably containing the B2 and bcc structures in addition to the D0<sub>3</sub> structure.

did not coexist with any other phases) by fitting our *P*-*V*-*T* data set to a Mie–Grüneisen equation of state

We determined a thermal equation of state for the hcp structure of this alloy (where it

$$P(V, T) = P_{300}(V) + \left(\frac{\gamma}{V}\right)[E(\theta_D, T) - E(\theta_D, 300)] \quad (2)$$

with the 300 K isothermal pressure (*P*<sub>300</sub>) described by the third-order Birch–Murnaghan equation of state (equation (1)) and the thermal pressure term based on a Debye model of vibrational energy (*E*), with Grüneisen parameter  $\gamma = \gamma_0(V/V_0)^q$  and Debye temperature  $\theta_D = \theta_0 \exp[\gamma_0(1 - (V/V_0)^q)/q]$ . We did not explicitly include any anharmonic or electronic contributions to the thermal pressure, instead allowing all thermal pressure variation to be described by  $\gamma$  and *q* [e.g., Fei et al., 2007; Fischer et al., 2011, 2012]. This reduced the number of fitted parameters, which was necessary in many cases given the resolution of our data. When we tried to fit to an additional electronic term, there was no improvement to the quality of the fit. Table 1 shows the equation of state parameters we found for the hcp structure of Fe–9Si. We fit *V*<sub>0</sub>, *K*<sub>0</sub>, *K*'<sub>0</sub>, and  $\gamma_0$ , fixing *q* at 1 and  $\theta_0$  to the value for iron [Dewaele et al., 2006]. Fixing certain terms in all of our equations of state was necessary, given the resolution of the data, and generally does not worsen the fit due to trade-offs between  $\gamma_0$  and *q* in describing the thermal pressure and the insensitivity of the fit to  $\theta_0$ . High-temperature isotherms calculated from our equation of state of hcp Fe–9Si are shown in Figure 2b. The pressure residuals of our hcp equation of state fit are shown in Figure S1b in the supporting information. They reach a maximum range of –2.9 to 2.7 GPa at ~200 GPa.

The equation of state of hcp Fe–9Si was the only one investigated at conditions producing observable nonhydrostatic stresses: we find no evidence for lattice-dependent strain anisotropy in any of our 300 K equations of state, at high temperatures (>2000 K), or at intermediate pressures (<150 GPa). At the most extreme strain conditions of this study (~200 GPa and <2000 K), we observe a maximum deviation in volume calculated from different peaks of ~0.12%. However, even when we corrected our volumes by this amount (an extreme end-member possibility), we did not observe significant changes in the fitted equation of state parameters.

**Table 1.** Equation of State Parameters for Various Phases of Fe–9Si Alloy, Compared to Results of Previous Studies<sup>a</sup>

Alloy and Reference	<i>V</i> <sub>0</sub> (cm <sup>3</sup> /mol Atoms)	<i>K</i> <sub>0</sub> (GPa)	<i>K</i> ' <sub>0</sub>	$\theta_0$ (K)	$\gamma_0$	<i>q</i>
D0 <sub>3</sub> Fe–9Si alloy (this study)	6.961 ± 0.012	183 ± 4	5.59 ± 0.51			
bcc-like Fe–8Si alloy [Lin et al., 2003]	6.986 ± 0.007	157.8 ± 4.0	5.26 ± 0.88			
bcc-like Fe–9Si alloy [Hirao et al., 2004]	6.924 ± 0.002	268 ± 5	5.3			
hcp Fe–9Si alloy (this study)	7.203 ± 0.054	129.1 ± 1.4	5.29 ± 0.08	417	1.14 ± 0.14	1
hcp Fe–8Si alloy [Lin et al., 2003]	6.882 ± 0.031	141 ± 10	5.70 ± 0.60			
hcp Fe–9Si alloy [Hirao et al., 2004]	6.71 ± 0.24	198 ± 9	4.7 ± 0.3			
hcp + B2 Fe–9Si alloy (this study)	6.905 ± 0.017	170.8 ± 1.6	4.49 ± 0.07	417	2.22 ± 0.08	1

<sup>a</sup>In this study, zero-pressure Debye temperatures ( $\theta_0$ ) were set to the value for iron [Dewaele et al., 2006], and entries with no stated uncertainties (and the zero-pressure volume of the D0<sub>3</sub> structure, which was measured experimentally) were held fixed in the fits. The bcc structure reported by other studies was most likely the D0<sub>3</sub> structure (see text for details).

Lin *et al.* [2003] and Hirao *et al.* [2004] determined room temperature equations of state of hcp Fe–7.9Si and Fe–8.7Si, respectively. Their equation of state parameters are listed in Table 1. The relatively high  $K_0$  reported by Hirao *et al.* [2004] can again be explained by nonhydrostatic conditions [Hirao *et al.*, 2004]. Trade-offs exist in the least squares fitting between  $V_0$ ,  $K_0$ , and  $K'_0$ , which could explain some of the variations between these three studies. The  $c/a$  ratio of the hcp phase of Fe–9Si is listed in Table S1 in the supporting information. This ratio decreases with pressure and generally increases with temperature within any given heating cycle in agreement with most previous experimental [e.g., Boehler *et al.*, 2008; Tateno *et al.*, 2010] and theoretical [e.g., Gannarelli *et al.*, 2005] works on pure hcp iron.

We also determined a thermal equation of state for the hcp + B2 mixture of Fe–9Si, approximating the bulk molar volume as the average of the volumes of the two phases and enlarging the uncertainty on the volume to incorporate the difference between those of the two phases [Fischer *et al.*, 2012]. It is not typical to construct an equation of state for a two-phase mixture, but in this case there was no better alternative, since we have no knowledge of how silicon partitioning between the two phases varies with pressure and temperature or of the relative abundances of the two phases. In addition, constructing an equation of state for the mixture is acceptable in this case, because the volume difference between the hcp and B2 phases is small (mean of  $0.3\% \pm 0.6\%$ ). The bulk molar volume is uncertain because we do not know the relative proportions of the two phases, but it must lie within this small range. The volume difference between hcp and B2 increases with pressure, however, so the equation of state should be extrapolated cautiously. The modal abundances of hcp and B2 are varying with pressure and partitioning silicon in such a way as to keep the bulk composition fixed. Finally, this approximation is validated by the fact that the goal is to make a comparison to the Earth's core (sections 5.2–5.4), near the conditions at which the data were collected. The fitted parameters representing 1 bar properties are less important than the mixture's properties under core conditions.

We fit our data on the hcp + B2 mixture of Fe–9Si to a Mie–Grüneisen equation of state as described above (equation (2)). The resulting equation of state parameters are listed in Table 1, and various isotherms calculated from these parameters are shown in Figure 2a. The pressure residuals of this equation of state are illustrated in Figure S1c in the supporting information. They reach minimum and maximum values of  $-5.9$  and  $6.4$  GPa, respectively. We fit  $V_0$ ,  $K_0$ ,  $K'_0$ , and  $\gamma_0$ , fixing  $q$  at 1 and  $\theta_0$  to the value for iron [Dewaele *et al.*, 2006]. We do not report an equation of state for the fcc + B2 mixture, due to the large volume difference between the two phases (mean of  $3.0\% \pm 2.7\%$ ).

We also fit our data for each phase of Fe–9Si to Vinet equations of state [Vinet *et al.*, 1987], as described in Text S1 in the supporting information. Table S4 in the supporting information lists the equation of state parameters we found for each phase using the Vinet equation. We followed the same procedure with the data on Fe–16Si from Fischer *et al.* [2012], listing those parameters in Table S5 in the supporting information. The Birch–Murnaghan fits are preferred due to their higher degree of self-consistency, as discussed in section 5 and in the supporting information.

## 4.2. Equations of State of FeSi

We fit our  $P$ - $V$  data set for stoichiometric B20 FeSi at room temperature to a third-order Birch–Murnaghan equation of state (equation (1)). The equation of state parameters we found for B20 FeSi are listed in Table 2. We fit  $K_0$  and  $K'_0$ , fixing the zero-pressure volume to the value we measured experimentally. A 300 K isotherm calculated from our equation of state for B20 FeSi can be seen in Figure 4. The pressure residuals to our fit can be found in Figure S2a in the supporting information. They range from  $-0.9$  to  $0.7$  GPa. The equation of state of B20 FeSi has previously been determined by Knittle and Williams [1995] and Lin *et al.* [2003] using diamond anvil cells, by Guyot *et al.* [1997] using a large volume press, and by Caracas and Wentzcovitch [2004] using ab initio methods. The equation of state parameters found by these previous studies are listed in Table 2.

We fit our  $P$ - $V$ - $T$  data set for B2 FeSi (where it did not coexist with B20 FeSi) to a Mie–Grüneisen equation of state (equation (2)). Table 2 shows the equation of state parameters we found. We fit  $K_0$ ,  $\gamma_0$ , and  $q$ .  $V_0$  was set to the value measured after decompression by Sata *et al.* [2010] and Ono *et al.* [2007],  $\theta_0$  was set to the value for iron [Dewaele *et al.*, 2006], and  $K'_0$  was set to the fitted value of Sata *et al.* [2010]. High-temperature isotherms calculated from our equation of state of B2 FeSi are shown in Figure 4. These pressure residuals are shown in Figure S2b in the supporting information. They span from  $-3.9$  to  $6.0$  GPa.

**Table 2.** Equation of State Parameters for the B20 and B2 Phases of Stoichiometric FeSi, Compared to Results of Previous Studies<sup>a</sup>

FeSi Phase and Reference	$V_0$ (cm <sup>3</sup> /mol Atoms)	$K_0$ (GPa)	$K'_0$	$\theta_0$ (K)	$\gamma_0$	$q$
B20 FeSi (this study)	6.803 ± 0.008	192.2 ± 1.6	5.03 ± 0.17			
B20 FeSi [Knittle and Williams, 1995]	6.701 ± 0.011	209 ± 6	3.5 ± 0.4			
B20 FeSi [Lin et al., 2003]	6.790 ± 0.007	184.7 ± 3.9	4.75 ± 0.37			
B20 FeSi [Guyot et al., 1997] <sup>b</sup>	6.804 ± 0.003	172 ± 3	4			
B20 FeSi [Caracas and Wentzcovitch, 2004] <sup>c</sup>	6.330	255	4.14			
B20 FeSi [Caracas and Wentzcovitch, 2004] <sup>d</sup>	6.788	221	4.18			
B2 FeSi (this study)	6.414	230.6 ± 1.8	4.17	417	1.30 ± 0.04	1.7 ± 0.2
B2 FeSi [Ono et al., 2007]	6.420 ± 0.009	225 ± 2	4			
B2 FeSi [Ono, 2013] <sup>e</sup>	6.423 ± 0.018	223.3 ± 8.7	5.50 ± 0.16			
B2 FeSi [Sata et al., 2010]	6.435	221.7 ± 3.2	4.167 ± 0.063			
B2 FeSi [Caracas and Wentzcovitch, 2004] <sup>c</sup>	5.901	262	4.55			
B2 FeSi [Caracas and Wentzcovitch, 2004] <sup>d</sup>	6.436	220	4.80			
B2 FeSi [Vočadlo et al., 1999] <sup>d</sup>	6.389	226	5.4			

<sup>a</sup>In this study, the zero-pressure Debye temperature ( $\theta_0$ ) for B2 FeSi was set to the value for iron [Dewaele et al., 2006] and  $V_0$  for B2 FeSi was set to its measured value after decompression [Ono et al., 2007; Sata et al., 2010], while  $K'_0$  was set to the fitted value of Sata et al. [2010]. Entries from this study with no stated uncertainties (and the zero-pressure volume of the B20 structure, which was measured experimentally) were held fixed in the fits.

<sup>b</sup>Other parameters reported:  $(\partial K/\partial T)_P = -0.043 \pm 0.008$  GPa/K and coefficient of thermal expansion  $\alpha = (5.1 \pm 0.4) \times 10^{-5}$  K<sup>-1</sup>.

<sup>c</sup>Local density approximation calculation.

<sup>d</sup>Generalized-gradient approximation calculation.

<sup>e</sup>Other parameters reported (ab initio):  $(\partial K/\partial T)_V = -0.00245 \pm 0.00023$  GPa/K and  $\alpha K_T(V_0, T) = 0.00710 \pm 0.00009$  GPa/K.

Ono et al. [2007], Ono [2013], and Sata et al. [2010] determined room temperature equations of state of B2 FeSi, laser annealing their samples with each compression step. The equation of state parameters they determined are also listed in Table 2. These previous studies all find similar values to the present result for  $K_0$ . Dobson et al. [2003] also determined a room temperature equation of state of B2 FeSi, but their sample was synthesized at 24 GPa and compressed only up to 40 GPa, so it may have been coexisting with a small amount of B20 FeSi [Fischer et al., 2013]. The equation of state of B2 FeSi has been determined computationally by Caracas and Wentzcovitch [2004] and Vočadlo et al. [1999] (Table 2).

In the range of ~13–41 GPa, where the B20 and B2 phases were coexisting, we did not use any of the  $P$ - $V$ - $T$  data in our equation of state fits, due to unknown silicon partitioning. We did not attempt to fit an equation of state to the B20 + B2 mixture, due to the relatively large volume difference between the two phases (mean of  $2.8\% \pm 1.5\%$ ). This volume difference is slightly smaller than that measured by Ono et al. [2007] (~4% at 25 GPa), possibly driven by the higher temperatures in our study.

We also fit our data for B20 FeSi and B2 FeSi to Vinet equations of state [Vinet et al., 1987]. Details and results of this fitting are described in the Text S1 in the supporting information. Table S6 in the supporting information lists the equation of state parameters we found for each phase by fitting to the Vinet equation.

## 5. Discussion

### 5.1. Comparison of Equations of State in the Fe-FeSi System

Fischer et al. [2012] report equations of state for Fe–16Si alloy in the D0<sub>3</sub> structure up to ~60 GPa and as an hcp + B2 mixture at higher pressures to ~140 GPa. Figure 6 compares room temperature equations of state of D0<sub>3</sub> Fe–9Si, D0<sub>3</sub> Fe–16Si, and B20 FeSi, plotting Eulerian strain  $f$  versus normalized stress  $F$ , where  $F = P/(3f[1 + 2f]^{5/2})$ . In this type of  $F$ - $f$  plot, a trend line through the data will have an intercept of  $K_0$  and a slope related to  $K'_0$  [Birch, 1978], with any curvature at high strain indicating the need for higher order terms in the equation of state fit. The close agreement between the data from all three alloys shows that their room temperature equations of state at high strains are very similar. This illustrates that silicon content does not have a strong impact on the compressibility of these alloys at high pressures and room temperature, similar to the observation of Lin et al. [2003]. Indeed, these room temperature equations of state all have very similar fitted values of the 1 bar bulk modulus, ranging from 183.0 GPa to 193.4 GPa. Their values of  $K'_0$  fall in the range 4.91–5.59 and are positively correlated with the measured 1 bar volumes. For comparison, hcp Fe has a  $K'_0$  of 5.38 for a fixed  $K_0$  of 163.4 GPa [Dewaele et al., 2006].

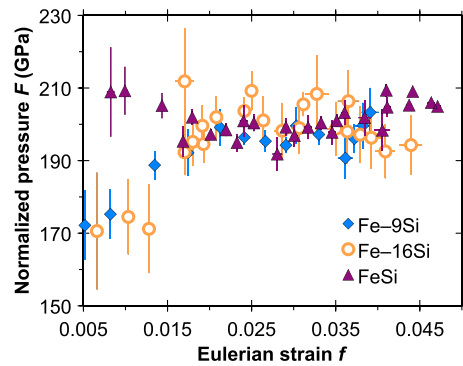
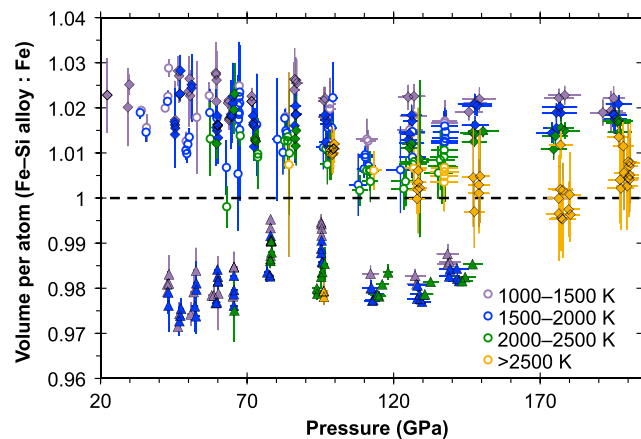


**Figure 6.**  $F$ - $f$  plot (normalized stress as a function of Eulerian strain) for various iron-silicon alloys at room temperature. Blue diamonds:  $D0_3$  Fe-9Si alloy (this study). Orange open circles:  $D0_3$  Fe-16Si [Fischer et al., 2012]. Purple triangles: B20 FeSi (this study).

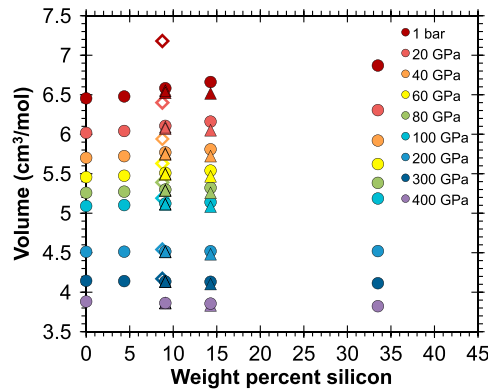
There is more variation in the equations of state of higher-pressure, high-temperature phases. The bulk modulus increases with increasing silicon content, while the 1 bar volume generally decreases. With  $q$  fixed at 1.0 in each equation of state,  $\gamma_0$  varies from 1.30 to 2.22.  $K'_0$  for B2 FeSi, hcp + B2 Fe-16Si, and hcp + B2 Fe-9Si are all in the range 4.0–4.5 while that of hcp Fe-9Si is 5.29, close to that of pure hcp iron [Dewaele et al., 2006]. A discussion of the differences and similarities between fits to the Birch-Murnaghan equation of state and the Vinet equation of state may be found in the supporting information.

Figure 7 illustrates the variation in volume per atom of iron-silicon alloys (compared to the volume per atom of pure iron) as a function of pressure and temperature. Volumes of iron were calculated at the same  $P$ - $T$  conditions as each data point using the equation of state of hcp Fe [Dewaele et al., 2006], for data in the stability field of hcp Fe, according to the iron phase diagram of Komabayashi and Fei [2010]. Data are shown for the B2 structure of FeSi (this study), the  $D0_3$  structure and average volume of an hcp + B2 mixture of Fe-16Si [Fischer et al., 2012], and the hcp structure and average volume of an hcp + B2 mixture of Fe-9Si (this study). The data vary with temperature, which is likely due to iron-silicon alloys having a different thermal expansion than pure iron. Another possibility is that this is an artifact of the form of the equation of state used. The equation of state of iron [Dewaele et al., 2006] includes harmonic, anharmonic, and electronic contributions to the thermal pressure, while the equations of state presented here (section 4) and in Fischer et al. [2012] fit only harmonic contributions.

At low pressures, silicon-bearing alloys Fe-9Si and Fe-16Si have a greater average distance between atoms relative to pure iron, but in stoichiometric FeSi this distance is smaller than in iron. At higher pressures and temperatures, these effects of silicon diminish. Figure 7 shows that as pressure and temperature increase toward the conditions of the Earth's core, the volume per atom of iron-silicon alloys relative to that of iron tends toward one. This trend holds for all three compositions shown here, even though data for different compositions follow different slopes, and for various crystal structures. Phase transitions generally have a smaller effect on the volume per atom than the silicon content does. This result suggests that iron and silicon atoms approach the same volume at deep Earth conditions and that density differences between various iron-silicon alloys at sufficiently high pressures are primarily due to differences in atomic mass.



**Figure 7.** Volume per atom of iron-silicon alloys (normalized to the volume of iron) as a function of pressure and temperature. Diamonds: hcp and hcp + B2 mixture of Fe-9Si alloy (this study). Open circles:  $D0_3$  and hcp + B2 mixture of Fe-16Si [Fischer et al., 2012]. Triangles: B2 FeSi (this study). All data are color coded by temperature according to the legend. Volumes of iron were calculated using the equation of state of Dewaele et al. [2006], and data are only shown for  $P$ - $T$  conditions under which the hcp structure of iron is stable [Komabayashi and Fei, 2010]. At very high pressures, data for all three compositions tend toward one (dashed line), suggesting that iron and silicon atoms approach the same volume at high  $P$ - $T$  conditions.



**Figure 8.** Ab initio  $P$ - $V$ - $X$  relationships in the Fe-FeSi system. Data shown are for pure iron,  $\text{Fe}_{11}\text{Si}$  (Fe-4Si),  $\text{Fe}_5\text{Si}$  (Fe-9Si),  $\text{Fe}_3\text{Si}$  (Fe-14Si), and stoichiometric FeSi (Fe-33Si) in the hcp crystal structure at 0 K, with data calculated from the experimentally determined equation of state of hcp Fe-9Si at 0 K shown for comparison. Filled circles: ordered structures. Filled triangles: disordered structures (with two different ordering schemes for Fe-9Si). Open diamonds: calculated from experimentally determined equation of state. Disordered structures have slightly smaller volumes than the ordered versions. Silicon increases the volumes of the alloys at low pressures but has little effect at high pressures. Volumes determined experimentally are higher than those obtained by computational methods at low pressures but agree at high pressures.

calculated from our experimentally determined equation of state (Table 1) for a temperature of 0 K. At low pressures, these volumes are larger than the ab initio volumes, with a higher compressibility. Both the volumes and compressibility determined by theory and experiment approximately converge at high pressures, showing agreement between the two methods.

Figure 9 shows  $F$ - $f$  plots of our ab initio data for the hcp structure at 0 K. Table 3 lists the isothermal (0 K) equation of state parameters for the ab initio results, based on linear fits to the data. The slopes of the data in Figure 9 change continuously with silicon content, with alloys with more silicon having lower slopes (lower  $K'_0$ ).

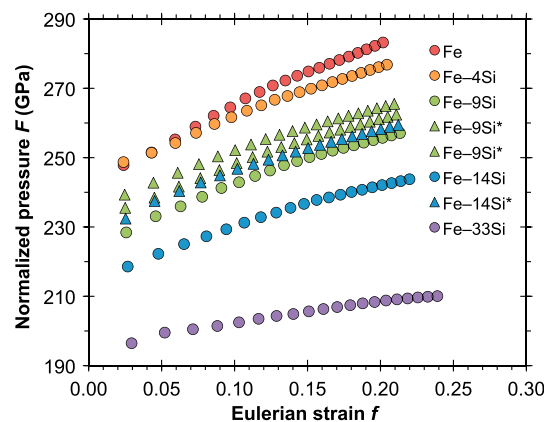


**Figure 9.**  $F$ - $f$  plot of our ab initio data on Fe,  $\text{Fe}_{11}\text{Si}$ ,  $\text{Fe}_5\text{Si}$ ,  $\text{Fe}_3\text{Si}$ , and FeSi in the hcp structure at 0 K up to 400 GPa. Circles: ordered structures. Triangles: disordered structures (with two different ordering schemes for Fe-9Si). Curvature in some of these trends may indicate the need for higher order terms in the equation of state fits.

Seagle *et al.* [2006] performed a similar analysis for  $\text{Fe}_3\text{S}$ , also finding that the volume per atom relative to iron tends toward one at high pressures, suggesting that iron, silicon, and sulfur atoms all have about the same effective volume in Fe-rich alloys at core conditions. This result supports, at least in these systems, a commonly held assumption that all atoms occupy similar volumes at high pressures. For example, this assumption was used by Birch [1952, 1964] to estimate the magnitude of the core density deficit and by McDonough [2003] to compute possible core compositions.

Figure 8 illustrates our ab initio  $P$ - $V$ - $X$  relationships for pure iron,  $\text{Fe}_{11}\text{Si}$  (Fe-4Si),  $\text{Fe}_5\text{Si}$  (Fe-9Si),  $\text{Fe}_3\text{Si}$  (Fe-14Si), and FeSi (Fe-33Si) at 0 K in the hcp structure. At low pressures, volume is an approximately linear function of silicon content, with silicon increasing the volume of the alloys. However, at higher pressures, this effect lessens, with all alloys converging to similar volumes by  $\sim 100$  GPa. This supports our result that iron and silicon atoms occupy approximately the same volume at high pressures, as seen in our experimental data (Figure 7). Results on a disordered structure of  $\text{Fe}_3\text{Si}$  and two disordered structures of  $\text{Fe}_5\text{Si}$  are also shown. These structures have slightly smaller volumes than their ordered counterparts, with this difference diminishing with increasing pressure.

Also shown in Figure 8 are  $P$ - $V$  data on hcp Fe-9Si, calculated from our experimentally determined equation of state (Table 1) for a temperature of 0 K. At low pressures, these volumes are larger than the ab initio volumes, with a higher compressibility. Both the volumes and compressibility determined by theory and experiment approximately converge at high pressures, showing agreement between the two methods.

This is consistent with the experimental data at room temperature on a variety of structures. Disordered structures exhibit slightly lower values of  $K'_0$  than ordered structures of the same composition. Figure 9 shows a variation in  $K'_0$  (intercept) with composition, with  $K'_0$  generally decreasing with increasing silicon content, which was not seen in the experimental data. Disordered structures have larger bulk moduli than ordered structures.

Our ab initio equation of state of pure hcp iron (Table 3) has a lower  $V_0$  (6.454 versus 6.753  $\text{cm}^3/\text{mol}$ ), higher  $K_0$  (244.5 versus 163.4 GPa), and lower  $K'_0$  (4.54 versus 5.38) compared to the experimentally determined equation of state of Dewaele *et al.* [2006]. The  $V_0$  fit to our experimental data on Fe-9Si (Table 1) is significantly larger than our ab initio  $V_0$  for ordered or disordered  $\text{Fe}_5\text{Si}$  (Table 3). The experimental data also show a lower bulk modulus and higher  $K'_0$  for Fe-9Si. These experimental

**Table 3.** Isothermal Equation of State Parameters for Iron-Silicon Alloys Based on Ab Initio Calculations at 0 K<sup>a</sup>

	$V_0$ (cm <sup>3</sup> /mol Atoms)	$K_0$ (GPa)	$K'_0$
Fe	6.454	244.5 ± 0.6	4.54 ± 0.01
Fe <sub>11</sub> Si	6.478	245.8 ± 0.4	4.45 ± 0.01
Fe <sub>5</sub> Si	6.583	227.1 ± 0.6	4.43 ± 0.01
Fe <sub>5</sub> Si*	6.524	237.5 ± 0.5	4.39 ± 0.01
Fe <sub>5</sub> Si*	6.552	233.1 ± 0.5	4.41 ± 0.01
Fe <sub>3</sub> Si	6.661	217.0 ± 0.5	4.39 ± 0.01
Fe <sub>3</sub> Si*	6.516	231.9 ± 0.6	4.39 ± 0.01
FeSi	6.870	196.0 ± 0.3	4.21 ± 0.01

<sup>a</sup>All alloys are in the hcp structure, with asterisks (\*) indicating disordered structures. Parameters were determined using *F-f* plots (Figure 9).

of Fe-Si alloys to that of iron [Dewaele et al., 2006] and the seismologically determined density of the core, such as in the PREM model [Dziewonski and Anderson, 1981]. For this analysis, we use a core-mantle boundary (CMB) pressure of 135.8 GPa and a density of 9.9 g/cm<sup>3</sup> in the outer core at the CMB [Dziewonski and Anderson, 1981]. The outer core temperature at the CMB is taken to be 4000 ± 500 K, based on the analysis of Anderson [2003]. We assume that the outer core temperature profile is adiabatic [Birch, 1952] and that iron and iron-rich alloys experience a 1–2% volume increase upon melting at core pressures [Anderson, 2003]. Although the outer core likely contains additional light elements, such as S, O, and/or C [e.g., McDonough, 2003], for this analysis we consider an outer core whose light element component consists of only silicon.

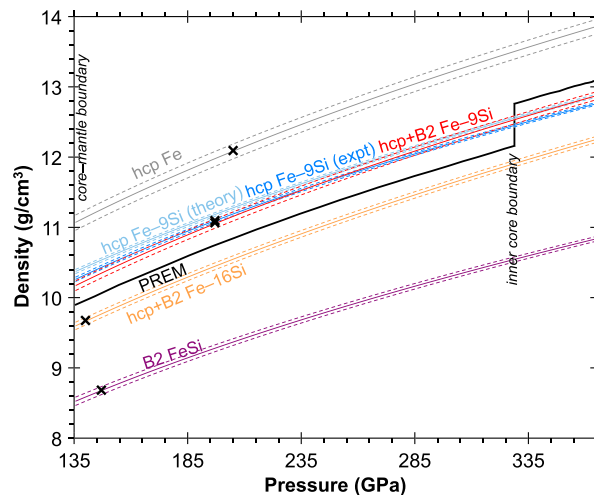


**Figure 10.** Evaluation of the core density deficit. Black curve: PREM [Dziewonski and Anderson, 1981]. Grey curve: density profile for solid hcp Fe, calculated from the equation of state of Dewaele et al. [2006]. Medium blue curve: density profile for solid hcp Fe–9Si, calculated from the experimentally determined equation of state parameters listed in Table 1. Light blue curve: profile for hcp Fe–9Si, calculated from the ab initio equation of state (Table 3) with temperature correction (see text for details). Red curve: density profile for hcp + B2 mixture of Fe–9Si, calculated from the equation of state parameters listed in Table 1. Orange curve: density profile for solid hcp + B2 mixture of Fe–16Si, from Fischer et al. [2012]. Purple curve: density profile for solid B2 FeSi, calculated from the equation of state parameters listed in Table 2. Solid curves follow an adiabatic temperature profile for a CMB temperature of 4000 K. Dashed curves indicate the effect of a 500 K uncertainty in the CMB temperature, which is a dominant source of uncertainty when evaluating the core density deficit. Black cross symbols: upper pressure limit of the experimental data coverage for each phase. As discussed in the text, these equations of state impose upper bounds of ~11 wt % Si in the outer core and 6–8 wt % Si in the inner core.

values are extrapolations of the fit to 1 bar, far from the *P-T* conditions of the data. At higher pressures, where the alloy was observed to have the hcp structure, the experimental and ab initio results are in closer agreement (Figure 8).

### 5.2. The Outer Core Density Deficit

Earth’s iron-rich core has a lower density than pure iron under the same *P-T* conditions [e.g., Birch, 1952]; this difference is known as the core density deficit. Assuming that the Earth’s core may be predominantly an iron-silicon alloy, we can place constraints on its silicon content by comparing our equations of state

of Fe-Si alloys to that of iron [Dewaele et al., 2006] and the seismologically determined density of the core, such as in the PREM model [Dziewonski and Anderson, 1981]. For this analysis, we use a core-mantle boundary (CMB) pressure of 135.8 GPa and a density of 9.9 g/cm<sup>3</sup> in the outer core at the CMB [Dziewonski and Anderson, 1981]. The outer core temperature at the CMB is taken to be 4000 ± 500 K, based on the analysis of Anderson [2003]. We assume that the outer core temperature profile is adiabatic [Birch, 1952] and that iron and iron-rich alloys experience a 1–2% volume increase upon melting at core pressures [Anderson, 2003]. Although the outer core likely contains additional light elements, such as S, O, and/or C [e.g., McDonough, 2003], for this analysis we consider an outer core whose light element component consists of only silicon.

Figure 10 illustrates the core density deficit, showing the density profile of pure solid hcp iron along a core adiabat [Dewaele et al., 2006] and PREM [Dziewonski and Anderson, 1981]. Based on the assumptions outlined above, PREM is 10.4 ± 0.9% less dense than solid hcp Fe at conditions of the CMB [Fischer et al., 2011, 2012]. Approximately 1–2% of this difference is due to the volume change of melting [Anderson, 2003], but the remainder of this deficit must be due to the presence of light elements in the outer core, such as silicon.

For the Fe–9Si alloy, we use the equation of state of the hcp structure to constrain the amount of silicon required to match the density deficit in the Earth’s core. This analysis requires no extrapolation in pressure and only a small extrapolation in temperature to apply our equation of state at CMB conditions. We corrected the outer core density to account for a Ni/Fe atomic ratio of 0.058 in the core [McDonough, 2003]. We find that a silicon content of 11.2 ± 0.7 wt % is required to match PREM in the outer core at the CMB for a purely Fe–Ni–Si outer core, based on the

**Table 4.** Weight Percent of Silicon Needed to Match the Density and Bulk Sound Speed of PREM [Dziewonski and Anderson, 1981] in the Inner and Outer Core, Determined for Each Iron-Silicon Alloy Investigated<sup>a</sup>

	Outer Core Density Deficit	Outer Core Bulk Sound Speed	Inner Core Density Deficit	Inner Core Bulk Sound Speed
Fe-9Si	11.2 ± 0.7	7.7 ± 1.8	6.0 ± 0.8	3.9 ± 0.2
Fe-16Si	11.3 ± 1.5	13.0 ± 1.9	7.7 ± 1.3	37 ± 9
FeSi	11.4 ± 1.6	9.0 ± 2.1	7.3 ± 1.4	9.2 ± 0.8
Weighted average	11.3 ± 0.6	9.9 ± 3.0	6.7 ± 1.1	4.2 ± 3.7
Fe-9Si (theory)	13.2 ± 0.9	4.5 ± 0.6	6.8 ± 0.8	5.0 ± 0.2

<sup>a</sup>Weighted averages only include calculations from experimentally determined equations of state and were calculated using equation (3). Value in italics was not used in determining the weighted average.

experimentally determined equation of state of Fe-9Si. The uncertainty in this calculation is based upon the stated uncertainties in the CMB temperature, the volume change upon melting, and the equation of state, with the uncertainties in CMB temperature and ΔV of melting dominating. Varying the amount of nickel in the core has very little effect on the amount of silicon needed to match PREM (less than ± 0.1 wt %). The density profile of Fe-9Si along a core adiabat is shown in Figure 10.

The light element component of Earth's core is likely to be comprised of multiple elements, so this calculation effectively provides the maximum amount of silicon that may exist in the Earth's outer core, with the remainder of the density deficit being comprised of other light elements. The eutectic composition in the Fe-Si system is less than 16 wt % Si at CMB conditions [Fischer et al., 2012, 2013]. A composition of 11.2 wt % silicon is consistent with this eutectic composition, because the coexisting solid phase (inner core) must be more Fe-rich. Assuming that this eutectic composition does not decrease dramatically at higher pressures, it is plausible on this basis that silicon could be the dominant light element in the Earth's core.

For stoichiometric FeSi, an analogous calculation can be performed using the equation of state of the B2 phase, which also requires no extrapolation in pressure to apply at CMB conditions. Following the same procedure, we find that a silicon content of 11.4 ± 1.6 wt % is required to match PREM in the outer core at the CMB for a purely Fe-Ni-Si outer core, based on the equation of state of FeSi. The density profile of FeSi at core conditions is shown in Figure 10.

Fischer et al. [2012] evaluated the core density deficit with regards to Fe-16Si, finding that 11.3 ± 1.5 wt % silicon is required to match PREM in the outer core at the CMB for a purely Fe-Ni-Si outer core. The density profile for an hcp + B2 mixture of Fe-16Si is also plotted in Figure 10 for reference. The maximum amounts of silicon in the outer core obtained by using each of these three equations of state (FeSi, Fe-9Si and Fe-16Si) agree, and a weighted mean μ\* can be calculated as follows:

$$\mu^* = \frac{\sum_{i=1}^n x_i}{\sum_{i=1}^n \frac{1}{\sigma_i^2}} \pm \sqrt{\frac{1}{\sum_{i=1}^n \frac{1}{\sigma_i^2}} + \frac{1}{n} \sum_{i=1}^n (x_i - \mu^*)^2} \quad (3)$$

where n is the number of values being averaged (n = 3), x<sub>i</sub> is the maximum amount of silicon in the core determined from each equation of state, and σ<sub>i</sub> is the uncertainty in each value. Here we have used a conservative calculation for the uncertainty on the weighted mean, incorporating both the uncertainties on the values being averaged (first term) and the standard deviation of the numbers being averaged (second term). The three equations of state give a weighted average value of 11.3 ± 0.6 wt % Si and are compared in Table 4. Results of the same calculation using the Vinet equation of state are similar and are shown in Table S7 in the supporting information, and density profiles of the alloys determined from their Vinet equation of state fits are shown in Figure S3.

Figure 10 also shows a density profile for hcp Fe-9Si calculated using our 0 K ab initio equation of state (Table 3) corrected for thermal pressure. We approximated thermal pressure as αK<sub>T</sub>ΔT determined from our experimentally determined equation of state for hcp Fe-9Si, where α is the coefficient of thermal expansion and K<sub>T</sub> is the isothermal bulk modulus, calculated as functions of pressure and temperature. The experimental and ab initio density profiles of hcp Fe-9Si are very close together and approximately parallel (Figure 10),

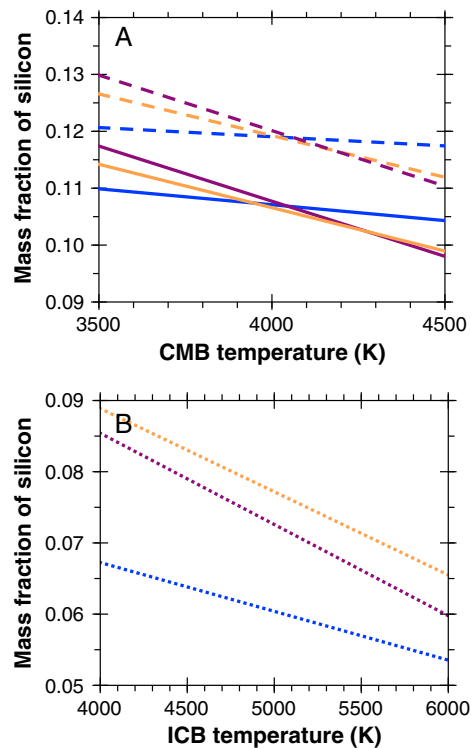


**Figure 11.** Trade-off between temperature and the amount of silicon required to match the density deficit of (a) the outer core and (b) the inner core for various iron-silicon alloys. Blue lines: hcp Fe-9Si alloy. Orange lines: hcp + B2 Fe-16Si. Purple lines: B2 FeSi. Dashed lines: 1% volume change upon melting. Solid lines: 2% volume change (density of the solid is shown). The outer core may contain up to ~11–12 wt % silicon, while the inner core may contain up to ~6–8 wt % silicon.

there is scatter in the data. A comparison to Figure S3 shows that the densities and bulk sound speeds of the alloys more closely approximate PREM and each other when the data are fit to Birch-Murnaghan equations of state, rather than to Vinet equations. We use the Birch-Murnaghan fits in this section, as discussed in the supporting information.

### 5.3. The Inner Core Density Deficit

The Earth's inner core is also less dense than pure iron under the same conditions. We assume an inner core boundary (ICB) temperature of  $5000 \pm 1000$  K [Boehler, 2000], pressure of 328.85 GPa, and density of the inner core of  $12.76 \text{ g/cm}^3$  at the ICB [Dziewonski and Anderson, 1981]. The density was again corrected for a Ni/Fe atomic ratio of 0.058 in the core [McDonough, 2003]. Based on these assumptions, PREM is  $5.7 \pm 0.8\%$  less dense than pure iron in the inner core at the ICB, with this density deficit caused by the presence of light elements in the inner core. Similar calculations to those done in section 5.2 can also be performed to assess the amount of silicon required to match the density deficit of the Earth's inner core. It should be cautioned that all of the calculations in this section require extrapolations in both pressure and temperature.

The density profiles of iron-rich Fe-Si alloys, compared to that of hcp Fe [Dewaele et al., 2006] and PREM [Dziewonski and Anderson, 1981], in the inner core are illustrated in Figure 10. Under the assumptions described above, for an Fe-Si-Ni inner core, the density deficit at the ICB can be explained by the presence of  $6.0 \pm 0.8$  wt % silicon in the inner core based on the equation of state of Fe-9Si, or  $7.3 \pm 1.4$  wt % silicon using the equation of state of FeSi. In comparison, Fischer et al. [2012] found a value of  $7.7 \pm 1.3$  wt % silicon using the equation of state of Fe-16Si (Table 4). These compositions are similar within uncertainty, yielding a weighted average of  $6.7 \pm 1.1$  wt % silicon using equation (3). It should be emphasized that this calculation

showing agreement between these methods. Our ab initio equation of state corrected for thermal pressure indicates a maximum silicon content of the outer core of  $13.2 \pm 0.9$  wt % Si, slightly larger than the values calculated from our experimentally determined equations of state (Table 4).

Figure 11a shows the trade-off between the core-mantle boundary temperature and the amount of silicon needed in the outer core at the CMB to match PREM for Fe-9Si, Fe-16Si, and FeSi. The greatest sources of uncertainty are the temperature of the core-mantle boundary and the volume change upon melting, though the equation of state chosen can also have significant effects. This figure illustrates that ~11–12 wt % silicon is needed to match the density deficit of the outer core.

Figure 10 shows that the density profiles of iron-silicon alloys with the most core relevant compositions (Fe-9Si and Fe-16Si) approximately match the slope of PREM when their equations of state are extrapolated through the *P-T* range of the Earth's outer core. This is not the case for density profiles of FeO [Fischer et al., 2011], Fe<sub>3</sub>S [Seagle et al., 2006], or Fe<sub>7</sub>C<sub>3</sub> [Nakajima et al., 2011] calculated from their equations of state. Huang et al. [2011] report density profiles of iron-oxygen-sulfur alloys, finding that only the most oxygen-poor alloys can match that of PREM. This lends support to the idea that silicon could be the dominant light element in the Earth's core. However, this comparison to PREM does require extrapolations in the equations of state of these alloys, and alternative explanations for variations in density profile slopes have been proposed [Fischer et al., 2011]. The density profiles of Fe-Si alloys from the shock wave study of Balchan and Cowan [1966] do not appear to match PREM well, though

requires large extrapolations in temperature, pressure, silicon content, and possibly crystal structure. Results of the same calculation using the Vinet equations of state are similar and are shown in Table S7 in the supporting information. Performing the same calculation using our ab initio equation of state corrected for thermal pressure (section 5.2) yields a maximum silicon content of the inner core of  $6.8 \pm 0.8$  wt % silicon, in agreement with the average value determined from the experimental equations of state (Table 4). The ab initio equation of state does not require any extrapolation in pressure to apply it to inner core boundary conditions. Its match to the experimental fit lends support to our calculations using extrapolated equations of state.

For Fe–9Si, the hcp + B2 mixture could be the stable phase at the inner core boundary, though the geotherm may lie near the hcp side of a wide two-phase loop [Fischer *et al.*, 2013]. Our present calculation may therefore be performed on a different phase of Fe–9Si alloy than would be found in the core. The transition from hcp to an hcp + B2 mixture is unlikely to have a very large effect on its density, since the relative proportions of hcp and B2 structures are changing gradually across the phase loop, which is expected to be very wide [Fischer *et al.*, 2013]. For stoichiometric FeSi, the stable phase at the ICB is predicted to be either the B2 phase [Brosh *et al.*, 2009; Zhang and Oganov, 2010] or an hcp + B2 mixture [Fischer *et al.*, 2013]. If a transition to an hcp + B2 mixture occurs in FeSi, it should again have a small effect on the density following the same logic as for Fe–9Si. Nevertheless, these extrapolations should be used with caution.

Figure 11b shows the relationship between the inner core boundary temperature and the amount of silicon required in the inner core to match the observed density deficit. Again, the variation in this number is controlled mostly by uncertainty in the ICB temperature, though the equation of state used is also important. This figure demonstrates that ~6–8 wt % silicon is needed to match PREM in the inner core.

This number can be compared to the amount of silicon needed to match the density deficit at the base of the outer core to determine the compositional contrast between the inner and outer core. The amount of silicon needed to match PREM in the outer core at the ICB is  $9.6 \pm 0.8$  wt % for Fe–9Si,  $10.3 \pm 1.1$  wt % for Fe–16Si, and  $11.4 \pm 1.2$  wt % for FeSi. This corresponds to a compositional contrast between the inner and outer core of  $3.6 \pm 1.2$  wt % Si,  $2.6 \pm 1.7$  wt % Si, and  $4.1 \pm 1.9$  wt % Si for Fe–9Si, Fe–16Si, and FeSi, respectively, or a weighted average of  $3.5 \pm 1.2$  wt % silicon by equation (3).

However, newer seismological models of the Earth's core generally report a larger density contrast at the ICB based on normal-mode seismology. Masters and Gubbins [2003] determined a contrast of  $0.82 \text{ g/cm}^3$  (versus  $0.60 \text{ g/cm}^3$  from PREM), which is primarily accommodated by a lower density at the base of the outer core. The amount of silicon needed to match this larger density contrast in the outer core at the ICB is  $11.7 \pm 0.8$  wt % for Fe–9Si,  $12.5 \pm 1.1$  wt % for Fe–16Si, and  $13.8 \pm 1.2$  wt % for FeSi. The larger light element content required to match the base of the outer core, relative to the top of the outer core calculated above, may reflect a light-element-enriched boundary layer near the ICB. Alternatively, this may be an artifact of the extrapolation required to meet the ICB conditions from our data set. This corresponds to a compositional contrast between the inner and outer core of  $5.7 \pm 1.2$  wt % Si,  $4.8 \pm 1.7$  wt % Si, and  $6.5 \pm 1.9$  wt % Si for Fe–9Si, Fe–16Si, and FeSi, respectively, or a weighted average of  $5.6 \pm 1.1$  wt % silicon by equation (3).

#### 5.4. Sound Velocities of Iron-Silicon Alloys

Earth's core has different sound wave velocities than pure iron under the same *P-T* conditions [e.g., Birch, 1964], with this difference caused by the presence of one or more light elements in the core. Comparison of the sound velocities of iron alloys to that of the core [Dziewonski and Anderson, 1981] can allow evaluation of the plausibility of various light element alloys as core candidates.

For this analysis, we use a bulk sound speed in the core at the CMB of  $8.07 \text{ km/s}$  [Dziewonski and Anderson, 1981], in addition to the other assumptions outlined in section 5.2. We calculated the bulk sound speed (equal to the *p* wave velocity  $V_p$  in the outer core) as the inverse square root of the slope of density versus pressure, determining this value numerically along adiabats in the outer core. Using the equation of state of hcp iron from Dewaele *et al.* [2006], we find that the bulk sound speed of pure iron in the outer core at the core-mantle boundary is  $7.81 \text{ km/s}$ . Figure 12 shows the bulk sound speed as a function of pressure through the Earth's outer core for pure hcp iron along a core adiabat [Dewaele *et al.*, 2006] and PREM [Dziewonski and Anderson, 1981]. The bulk sound speed of iron is  $3.2 \pm 0.2\%$  lower than that of PREM at conditions of the core-mantle boundary. Applying a fixed  $\Delta V$  of melting to extrapolate this calculation to the liquid state (section 5.2) has no effect on the calculated sound velocity, so this discrepancy must be due to the presence of light

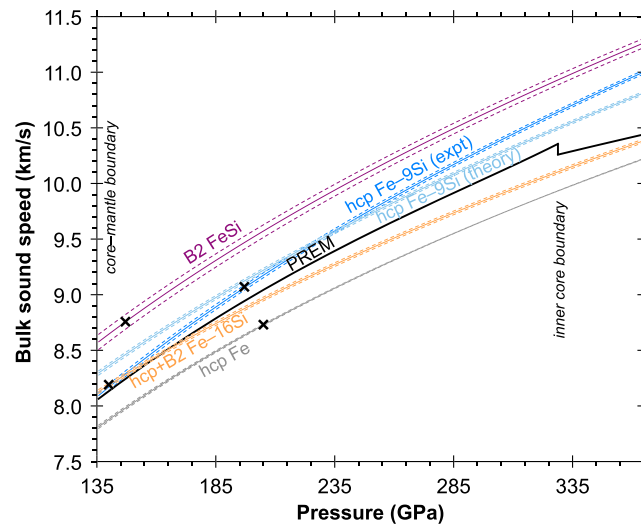


**Figure 12.** Comparison of equations of state of Fe-Si alloys to the bulk sound speed of the core. Curves are calculated from the same equations of state as indicated in the caption for Figure 10. Black cross symbols: upper pressure limit of the experimental data coverage for each phase. As discussed in the text, these curves suggest an outer core composition of ~8–13 wt % silicon and an inner core composition of 4–9 wt % Si.

elements, such as silicon, in the outer core. The sound speed of iron at core conditions calculated from the equation of state of *Dewaele et al.* [2006] is very insensitive to temperature (Figure 12).

Performing this calculation using the equations of state for our alloys, we find that the amount of silicon needed in the outer core at the CMB to match the observed bulk sound velocity is  $9.9 \pm 3.0$  wt % (weighted average of results using different equations of state from equation (3); Table 4). This number is in approximate agreement with the amount of silicon needed to match the density deficit at the CMB (section 5.2), which strengthens the possibility that silicon could be the primary light element in the Earth's core. The bulk sound speed profiles of these three alloys along core adiabats are illustrated in Figure 12. The slopes do not very precisely match PREM, in agreement with the shock wave data of *Balchan and Cowan* [1966], but the slopes vary, suggesting poor extrapolations and that the derivative of bulk sound speed with respect to pressure is not well constrained by our data. *Huang et al.* [2011] measured sound velocities as a function of density for Fe-O-S alloys in shock experiments, reporting that only sulfur-rich, oxygen-poor alloys could match the sound speed profile of PREM.

Our ab initio equation of state of Fe-9Si does a much better job of reproducing the bulk sound speed profile of PREM in the outer core than the experimentally determined equations of state (Figure 12). However, using our ab initio equation of state, we find that the maximum amount of silicon in the outer core is  $4.5 \pm 0.6$  wt % Si (Table 4). This number is significantly smaller than that calculated from the experimentally determined equations of state, or from comparison of the ab initio equation of state to the density deficit (section 5.2).

An analogous calculation may be performed for the Earth's inner core, comparing the seismic velocities at the inner core boundary. The bulk sound speed of the inner core at the ICB is 10.26 km/s from PREM [*Dziewonski and Anderson*, 1981] while that of iron under the same conditions is approximately 3.3% lower. We find that the amount of silicon needed to match the core's bulk sound speed ranges from ~4 to 9 wt % silicon, using the equations of state of Fe-9Si and FeSi (Table 4). This value encompasses the amount of silicon needed to match the inner core density deficit, 6.7 wt % (section 5.3). The ab initio equation of state of Fe-9Si gives a value of  $5.0 \pm 0.2$  wt % Si (Table 4). In general, the ab initio equation of state agrees better with the experimentally determined equations of state at higher pressures (i.e., inner core calculations).

The bulk sound speeds of iron, PREM, Fe-9Si, Fe-16Si, and FeSi are compared in Figure 12. The equation of state of Fe-16Si yielded an unrealistically high value for the amount of silicon needed to match the bulk sound speed of the inner core (37 wt %), possibly due to the fact that  $K'_0$  was fixed to a value of four in its equation of state, or because the fit of its equation of state to the average volume of a two-phase mixture [*Fischer et al.*, 2012] was unable to accurately describe silicon partitioning at such highly extrapolated pressures

and temperatures. The slope of the bulk sound speed profile for Fe–16Si is different from those of the other alloys and PREM [Dziewonski and Anderson, 1981] (Figure 12), illustrating a problem with the extrapolation of its equation of state.

Results of the same calculations for the outer and inner core using the Vinet equation of state are shown in Table S7 in the supporting information, and sound speed profiles of the alloys determined from their Vinet equation of state fits are shown in Figure S4. These profiles are very inconsistent with PREM, and the calculations yield conflicting and implausible answers. This indicates that either the Vinet equation fits to our data do not extrapolate as well as the Birch–Murnaghan fits, contrary to the findings of Cohen *et al.* [2000], or that silicon is not the dominant light element in the Earth's core.

Mao *et al.* [2012] measured sound velocities in iron and iron-silicon alloys, investigating their  $V_p$ - $\rho$  relationship using inelastic X-ray scattering and X-ray diffraction. They concluded that an alloy containing 8 wt % silicon at 6000 K matches well with PREM [Dziewonski and Anderson, 1981] in the inner core. This result is in agreement with our estimate of the silicon content of the inner core of 6–8 wt % based on the density deficit (section 5.3). Antonangeli *et al.* [2010] performed similar experiments on an iron-nickel-silicon alloy, finding that only 1–2 wt % silicon is required to match PREM. Badro *et al.* [2007] measured sound velocities of FeSi, finding a preferred model for the inner core containing 2.3 wt % silicon and traces of oxygen.

## 6. Conclusions

The equations of state of the D0<sub>3</sub> phase of Fe–9Si and the B20 phase of stoichiometric FeSi were measured to high pressures at room temperature. Those of the hcp + B2 mixture and the hcp phase of Fe–9Si were determined to ~200 GPa and high temperatures while that of B2 FeSi was measured to ~145 GPa and high temperatures. Comparing these results with the equations of state of Fe–16Si [Fischer *et al.*, 2012] and hcp iron [Dewaele *et al.*, 2006] shows that silicon does not have a strong effect on compressibility of iron-silicon alloys and that silicon and iron have similar volumes per atom at megabar pressures. Equations of state of Fe, Fe<sub>11</sub>Si, Fe<sub>5</sub>Si, Fe<sub>3</sub>Si, and FeSi have been calculated using ab initio methods, which agree with the experimental results at high pressures.

Using these equations of state of Fe–9Si and FeSi, Fe–16Si [Fischer *et al.*, 2012], and hcp iron [Dewaele *et al.*, 2006], we have made comparisons to PREM [Dziewonski and Anderson, 1981] to evaluate the amount of silicon that could be in the Earth's core. Based on comparisons to the observed core density deficit, we find that the maximum amount of silicon in the outer core is ~11 wt %, while the maximum amount in the inner core is 6–8 wt %, for a purely Fe–Si–Ni core. Comparing the bulk sound speed of PREM with those calculated from the equations of state of iron-silicon alloys suggest an outer core composition of ~8–13 wt % silicon, and an inner core composition of ~4–9 wt % silicon. The compositional contrast between the inner and outer core is found to be  $3.5 \pm 1.2$  wt % silicon by matching PREM or  $5.6 \pm 1.2$  wt % Si matching Masters and Gubbins [2003]. Equations of state of various iron-silicon alloys typically give similar results for silicon contents of the core and provide a good match to PREM in terms of density, sound speed, and density variations with depth, suggesting that silicon is a viable candidate for the dominant light element in the Earth's core.

## References

- Ahrens, T. J. (1982), Constraints on core composition from shock-wave data, *Phil. Trans. R. Soc. London A*, *306*, 37–47.
- Allègre, C. J., J.-P. Poirier, E. Humler, and A. W. Hofmann (1995), The chemical composition of the Earth, *Earth Planet. Sci. Lett.*, *134*, 515–526.
- Anderson, O. L. (2003), The three-dimensional phase diagram of iron, in *Earth's Core: Dynamics, Structure, Rotation*, edited by V. Dehant *et al.*, pp. 83–103, AGU, Washington, D. C.
- Antonangeli, D., J. Siebert, J. Badro, D. L. Farber, G. Fiquet, G. Morard, and F. J. Ryerson (2010), Composition of the Earth's inner core from high-pressure sound velocity measurements in Fe–Ni–Si alloys, *Earth Planet. Sci. Lett.*, *295*, 292–296, doi:10.1016/j.epsl.2010.04.018.
- Badro, J., G. Fiquet, F. Guyot, E. Gregoryanz, F. Occelli, D. Antonangeli, and M. d'Astuto (2007), Effect of light elements on the sound velocities in solid iron: Implications for the composition of Earth's core, *Earth Planet. Sci. Lett.*, *254*, 233–238, doi:10.1016/j.epsl.2006.11.025.
- Balchan, A. S., and G. R. Cowan (1966), Shock compression of two iron–silicon alloys to 2.7 megabars, *J. Geophys. Res.*, *71*, 3577–3588.
- Birch, F. (1952), Elasticity and constitution of the Earth's interior, *J. Geophys. Res.*, *37*, 227–286.
- Birch, F. (1964), Density and composition of mantle and core, *J. Geophys. Res.*, *69*, 4377–4388.
- Birch, F. (1978), Finite strain isotherm and velocities for single-crystal and polycrystalline NaCl at high pressures and 300°K, *J. Geophys. Res.*, *83*, 1257–1268.
- Blöchl, P. E. (1994), Projector augmented-wave method, *Phys. Rev. B*, *50*, 17,953–17,979.
- Boehler, R. (2000), High-pressure experiments and the phase diagram of lower mantle and core materials, *Rev. Geophys.*, *38*, 221–245.
- Boehler, R., D. Santamaría-Pérez, D. Errandonea, and M. Mezouar (2008), Melting, density, and anisotropy of iron at core conditions: New X-ray measurements to 150 GPa, *J. Phys. Conf. Ser.*, *121*, 022018, doi:10.1088/1742-6596/121/2/022018.

### Acknowledgments

We thank the Editor for handling our submission and two anonymous reviewers for helping to improve the manuscript. We acknowledge beamline scientists Jason Knight, Alastair MacDowell, and Jinyuan Yan, who helped us during this project. We thank Gwen Gage and Bethany Chidester for their assistance at the beamline, Maria Valdes for help with sample preparation, and Sergey Tkachev for assistance with gas loading. This material is based upon work supported by a National Science Foundation (NSF) Graduate Research Fellowship, an Illinois Space Grant Consortium Fellowship, and a Ludo Frevel Crystallography Scholarship to R.A.F. This work was also supported by the NSF by grant EAR-1243847 to A.J.C., and grant EAR-0944298 to D.L.H. R.C. acknowledges support from the Rhone-Alpes region in the CIBLE 2010 framework. The ab initio calculations have been performed on the Jade machine of CINES and the Curie machine of CCRT under DARI computational grant x2013106368. Portions of this work were performed at GeoSoilEnviroCARS (Sector 13), Advanced Photon Source (APS), Argonne National Laboratory. GeoSoilEnviroCARS is supported by the NSF Earth Sciences (EAR-0622171) and Department of Energy (DOE) Geosciences (DE-FG02-94ER14466). Use of the APS was supported by the U.S. DOE, Office of Science, Office of Basic Energy Sciences, under contract DE-AC02-06CH11357. This research was partially supported by COMPRES, the Consortium for Materials Properties Research in Earth Sciences under NSF Cooperative Agreement EAR 10-43050. The Advanced Light Source is supported by the Director, Office of Science, Office of Basic Energy Sciences, of the U.S. DOE under contract DE-AC02-05CH11231.

- Brosh, E., G. Makov, and R. Z. Shneck (2009), Thermodynamic analysis of high-pressure phase equilibria in Fe–Si alloys, implications for the inner-core, *Phys. Earth Planet. Int.*, *172*, 289–298, doi:10.1016/j.pepi.2008.10.012.
- Campbell, A. J., C. T. Seagle, D. L. Heinz, G. Shen, and V. B. Prakapenka (2007), Partial melting in the iron–sulfur system at high pressure: A synchrotron X-ray diffraction study, *Phys. Earth Planet. Int.*, *162*, 119–128, doi:10.1016/j.pepi.2007.04.001.
- Campbell, A. J., L. Danielson, K. Righter, C. T. Seagle, Y. Wang, and V. B. Prakapenka (2009), High pressure effects on the iron–iron oxide and nickel–nickel oxide oxygen fugacity buffers, *Earth Planet. Sci. Lett.*, *286*, 556–564, doi:10.1016/j.epsl.2009.07.022.
- Caracas, R., and R. Wentzcovitch (2004), Equation of state and elasticity of FeSi, *Geophys. Res. Lett.*, *31*, L20603, doi:10.1029/2004GL020601.
- Chabot, N. L., W. F. McDonough, J. H. Jones, S. A. Saslow, R. D. Ash, D. S. Draper, and C. B. Agee (2011), Partitioning behavior at 9 GPa in the Fe–S system and implications for planetary evolution, *Earth Planet. Sci. Lett.*, *305*, 425–434, doi:10.1016/j.epsl.2011.03.027.
- Cohen, R. E., O. Gülseren, and R. J. Hemley (2000), Accuracy of equation-of-state formulations, *Am. Mineral.*, *85*, 338–344.
- Deguen, R. (2012), Structure and dynamics of Earth's inner core, *Earth Planet. Sci. Lett.*, *333–334*, 211–225, doi:10.1016/j.epsl.2012.04.038.
- Dewaele, A., P. Loubeyre, F. Occelli, M. Mezouar, P. I. Dorogokupets, and M. Torrent (2006), Quasihydrostatic equation of state of iron above 2 Mbar, *Phys. Rev. Lett.*, *97*, 215504, doi:10.1103/PhysRevLett.97.215504.
- Dobson, D. P., L. Vočadlo, and I. G. Wood (2002), A new high-pressure phase of FeSi, *Am. Mineral.*, *87*, 784–787.
- Dobson, D. P., W. A. Crichton, P. Bouvier, L. Vočadlo, and I. G. Wood (2003), The equation of state of CsCl-structured FeSi to 40 GPa: Implications for silicon in the Earth's core, *Geophys. Res. Lett.*, *30*(1), 1014, doi:10.1029/2002GL016228.
- Dziewonski, A. M., and D. L. Anderson (1981), Preliminary reference Earth model, *Phys. Earth Planet. Inter.*, *25*, 297–356.
- Fei, Y., A. Ricolleau, M. Frank, K. Mibe, G. Shen, and V. Prakapenka (2007), Toward an internally consistent pressure scale, *Proc. Natl. Acad. Sci. U.S.A.*, *104*, 9182–9186, doi:10.1073/pnas.0609013104.
- Fischer, R. A., A. J. Campbell, G. A. Shofner, O. T. Lord, P. Dera, and V. B. Prakapenka (2011), Equation of state and phase diagram of FeO, *Earth Planet. Sci. Lett.*, *304*, 496–502, doi:10.1016/j.epsl.2011.02.025.
- Fischer, R. A., A. J. Campbell, R. Caracas, D. M. Reaman, P. Dera, and V. B. Prakapenka (2012), Equation of state and phase diagram of Fe–16Si alloy as a candidate component of Earth's core, *Earth Planet. Sci. Lett.*, *357–358*, 268–276, doi:10.1016/j.epsl.2012.09.022.
- Fischer, R. A., A. J. Campbell, D. M. Reaman, N. A. Miller, D. L. Heinz, P. Dera, and V. B. Prakapenka (2013), Phase relations in the Fe–FeSi system at high pressures and temperatures, *Earth Planet. Sci. Lett.*, *373*, 54–64, doi:10.1016/j.epsl.2013.04.035.
- Fitoussi, C., B. Bourdon, T. Kleine, F. Oberli, and B. C. Reynolds (2009), Si isotope systematic of meteorites and terrestrial peridotites: Implications for Mg/Si fractionation in the solar nebula and for Si in the Earth's core, *Earth Planet. Sci. Lett.*, *287*, 77–85, doi:10.1016/j.epsl.2009.07.038.
- Gannarelli, C. M. S., D. Alfè, and M. J. Gillan (2005), The axial ratio of hcp iron at the conditions of the Earth's inner core, *Phys. Earth Planet. Inter.*, *152*, 67–77, doi:10.1016/j.pepi.2005.06.003.
- Georg, R. B., A. N. Halliday, E. A. Schauble, and B. C. Reynolds (2007), Silicon in the Earth's core, *Nature*, *447*, 1102–1106, doi:10.1038/nature05927.
- Gonze, X., et al. (2002), First-principles computation of material properties: The ABINIT software project, *Comput. Mater. Sci.*, *25*, 478–492.
- Gonze, X., et al. (2009), ABINIT: First-principles approach to material and nanosystem properties, *Comp. Phys. Comm.*, *180*, 2582–2816, doi:10.1016/j.cpc.2009.07.007.
- Guyot, F., J. Zhang, I. Martinez, J. Matas, Y. Ricard, and M. Javoy (1997), P-V-T measurements of iron silicide ( $\epsilon$ -FeSi): Implications for silicate-metal interactions in the early Earth, *Eur. J. Mineral.*, *9*, 277–285.
- Hammersley, A. P., S. O. Svensson, M. Hanfland, A. N. Fitch, and D. Häusermann (1996), Two-dimensional detector software: From real detector to idealized image or two-theta scan, *High Pressure Res.*, *14*, 235–248.
- Hirao, N., E. Ohtani, T. Kondo, and T. Kikegawa (2004), Equation of state of iron–silicon alloys to megabar pressure, *Phys. Chem. Minerals*, *31*, 329–336, doi:10.1007/s00269-004-0387-x.
- Huang, H., Y. Fei, L. Cai, F. Jing, X. Hu, H. Xie, L. Zhang, and Z. Gong (2011), Evidence for an oxygen-depleted liquid outer core of the Earth, *Nature*, *479*, 513–516, doi:10.1038/nature10621.
- Javoy, M., et al. (2010), The chemical composition of the Earth: Enstatite chondrite models, *Earth Planet. Sci. Lett.*, *293*, 259–268, doi:10.1016/j.epsl.2010.02.033.
- Knittle, E., and R. Jeanloz (1991), Earth's core–mantle boundary: Results of experiments at high pressures and temperatures, *Science*, *251*, 1438–1443.
- Knittle, E., and Q. Williams (1995), Static compression of  $\epsilon$ -FeSi and an evaluation of reduced silicon as a deep Earth constituent, *Geophys. Res. Lett.*, *22*, 445–448.
- Komabayashi, T., and Y. Fei (2010), Internally consistent thermodynamic database for iron to the Earth's core conditions, *J. Geophys. Res.*, *115*, B03202, doi:10.1029/2009JB006442.
- Kunz, M., et al. (2005), A beamline for high-pressure studies at the Advanced Light Source with a superconducting bending magnet as the source, *J. Synchrotron Rad.*, *12*, 650–658, doi:10.1107/S0909049505020959.
- Kuwayama, Y., T. Sawai, K. Hirose, N. Sata, and Y. Ohishi (2009), Phase relations of iron–silicon alloys at high pressure and high temperature, *Phys. Chem. Minerals*, *36*, 511–518, doi:10.1007/s00269-009-0296-0.
- Lin, J.-F., D. L. Heinz, A. J. Campbell, J. M. Devine, and G. Shen (2002), Iron–silicon alloy in Earth's core?, *Science*, *295*, 313–315.
- Lin, J.-F., A. J. Campbell, D. L. Heinz, and G. Shen (2003), Static compression of iron–silicon alloys: Implications for silicon in the Earth's core, *J. Geophys. Res.*, *108*(B1), 2045, doi:10.1029/2002JB001978.
- Lin, J.-F., H. P. Scott, R. A. Fischer, Y.-Y. Chang, I. Kantor, and V. B. Prakapenka (2009), Phase relations of Fe–Si alloy in Earth's core, *Geophys. Res. Lett.*, *36*, L06306, doi:10.1029/2008GL036990.
- Lord, O. T., M. J. Walter, D. P. Dobson, L. Armstrong, S. M. Clark, and A. Kleppe (2010), The FeSi phase diagram to 150 GPa, *J. Geophys. Res.*, *115*, B06208, doi:10.1029/2009JB006528.
- Mao, H. K., J. Xu, and P. M. Bell (1986), Calibration of the ruby pressure gauge to 800 kbar under quasi-hydrostatic conditions, *J. Geophys. Res.*, *91*, 4673–4676.
- Mao, Z., J.-F. Lin, J. Liu, A. Alatas, L. Gao, J. Zhao, and H.-K. Mao (2012), Sound velocities of Fe and Fe–Si alloy in the Earth's core, *Proc. Natl. Acad. Sci. U.S.A.*, *109*, 10,239–10,244, doi:10.1073/pnas.1207086109.
- Massalski, T. B. (1986), *Binary Alloy Phase Diagrams*, American Society for Metals, Metals Park, Ohio.
- Masters, G., and D. Gubbins (2003), On the resolution of density within the Earth, *Phys. Earth Planet. Int.*, *140*, 159–167, doi:10.1016/j.pepi.2003.07.008.
- McDonough, W. F. (2003), Compositional model for the Earth's core, in *Treatise of Geochemistry*, vol. 2, edited by R. W. Carlson, pp. 547–568, Elsevier-Perigamon, Oxford, U. K.
- Miller, N. A. (2009), Melting and phase relations in iron–silicon alloys with applications to the Earth's core (MS thesis), University of Maryland, College Park, Md.
- Morard, G., D. Andraut, N. Guignot, J. Siebert, G. Garbarino, and D. Antonangeli (2011), Melting of Fe–Ni–Si and Fe–Ni–S alloys at megabar pressures: Implications for the core–mantle boundary temperature, *Phys. Chem. Minerals*, *38*, 767–776, doi:10.1007/s00269-011-0449-9.

- Nakajima, Y., E. Takahashi, N. Sata, Y. Nishihara, K. Hirose, K. Funakoshi, and Y. Ohishi (2011), Thermoelastic properties and high-pressure stability of  $\text{Fe}_7\text{C}_3$ : Implications for iron-carbide in the Earth's core, *Am. Mineral.*, *96*, 1158–1165, doi:10.2138/am.2011.3703.
- Ono, S., T. Kikegawa, and Y. Ohishi (2007), Equation of state of the high-pressure polymorph of FeSi to 67 GPa, *Eur. J. Mineral.*, *19*, 183–187, doi:10.1127/0935-1221/2007/0019-1713.
- Ono, S. (2013), Equation of state and elasticity of B2-type FeSi: Implications for silicon in the inner core, *Phys. Earth Planet. Inter.*, *224*, 32–37, doi:10.1016/j.pepi.2013.08.009.
- Ozawa, H., K. Hirose, M. Mitome, Y. Bando, N. Sata, and Y. Ohishi (2008), Chemical equilibrium between ferropericlasite and molten iron to 134 GPa and implications for iron content at the bottom of the mantle, *Geophys. Res. Lett.*, *35*, L05308, doi:10.1029/2007GL032648.
- Ozawa, H., K. Hirose, M. Mitome, Y. Bando, N. Sata, and Y. Ohishi (2009), Experimental study of reaction between perovskite and molten iron to 146 GPa and implications for chemically distinct buoyant layer at the top of the core, *Phys. Chem. Minerals*, *36*, 355–363, doi:10.1007/s00269-008-0283-x.
- Perdew, J. P., K. Burke, and M. Ernzerhof (1996), Generalized gradient approximation made simple, *Phys. Rev. Lett.*, *77*, 3865–3868.
- Prakapenka, V. B., A. Kuba, A. Kuznetsov, A. Laskin, O. Shkurikhin, P. Dera, M. L. Rivers, and S. R. Sutton (2008), Advanced flat top laser heating system for high pressure research at GSECARS: Application to the melting behavior of germanium, *High Pressure Res.*, *28*, 225–235, doi:10.1080/089579508020507.
- Ricolleau, A., Y. Fei, A. Corgne, J. Siebert, and J. Badro (2011), Oxygen and silicon contents of Earth's core from high pressure metal–silicate partitioning experiments, *Earth Planet. Sci. Lett.*, *310*, 409–421, doi:10.1016/j.epsl.2011.08.004.
- Righter, K. (2011), Prediction of metal–silicate partition coefficients for siderophile elements: An update and assessment of PT conditions for metal–silicate equilibrium during accretion of the Earth, *Earth Planet. Sci. Lett.*, *304*, 158–167, doi:10.1016/j.epsl.2011.01.028.
- Ringwood, A. E. (1959), On the chemical evolution and densities of the planets, *Geochim. Cosmochim. Acta*, *15*, 257–283.
- Rivers, M., V. B. Prakapenka, A. Kubo, C. Pullins, C. M. Holl, and S. D. Jacobsen (2008), The COMPRES/GSECARS gas-loading system for diamond anvil cells at the Advanced Photon Source, *High Pressure Res.*, *28*, 273–292, doi:10.1080/08957950802333593.
- Rubie, D. C., D. J. Frost, U. Mann, Y. Asahara, F. Nimmo, K. Tsuno, P. Kegler, A. Holzheid, and H. Palme (2011), Heterogeneous accretion, composition and core–mantle differentiation of the Earth, *Earth Planet. Sci. Lett.*, *301*, 31–42, doi:10.1016/j.epsl.2010.11.030.
- Santamaría-Pérez, D., and R. Boehler (2008), FeSi melting curve up to 70 GPa, *Earth Planet. Sci. Lett.*, *265*, 743–747, doi:10.1016/j.epsl.2007.11.008.
- Sata, N., K. Hirose, G. Shen, Y. Nakajima, Y. Ohishi, and N. Hirao (2010), Compression of FeSi,  $\text{Fe}_3\text{C}$ ,  $\text{Fe}_{0.95}\text{O}$ , and FeS under the core pressures and implication for light element in the Earth's core, *J. Geophys. Res.*, *115*, B09204, doi:10.1029/2009JB006975.
- Seagle, C. T., A. J. Campbell, D. L. Heinz, G. Shen, and V. B. Prakapenka (2006), Thermal equation of state of  $\text{Fe}_3\text{S}$  and implications for sulfur in Earth's core, *J. Geophys. Res.*, *111*, B06209, doi:10.1029/2005JB004091.
- Shahar, A., K. Ziegler, E. D. Young, A. Ricolleau, E. A. Schauble, and Y. Fei (2009), Experimentally determined Si isotope fractionation between silicate and Fe metal and implications for Earth's core formation, *Earth Planet. Sci. Lett.*, *288*, 228–234, doi:10.1016/j.epsl.2009.09.025.
- Shen, G., M. L. Rivers, Y. Wang, and S. R. Sutton (2001), Laser heated diamond cell system at the Advanced Photon Source for in situ measurements at high pressure and temperature, *Rev. Sci. Instrum.*, *72*, 1273–1282.
- Shen, G., M. L. Rivers, Y. Wang, and S. R. Sutton (2005), Facilities for high-pressure research with the diamond anvil cell at GSECARS, *J. Synchrotron Rad.*, *12*, 642–649, doi:10.1107/S0909049505022442.
- Siebert, J., J. Badro, D. Antonangeli, and F. J. Ryerson (2012), Metal–silicate partitioning of Ni and Co in a deep magma ocean, *Earth Planet. Sci. Lett.*, *321–322*, 189–197, doi:10.1016/j.epsl.2012.01.013.
- Stevenson, D. L. (1981), Models of the Earth's core, *Science*, *214*, 611–619.
- Takafuji, N., K. Hirose, M. Mitome, and Y. Bando (2005), Solubilities of O and Si in liquid iron in equilibrium with  $(\text{Mg},\text{Fe})\text{SiO}_3$  perovskite and the light elements in the core, *Geophys. Res. Lett.*, *32*, L06313, doi:10.1029/2005GL022773.
- Tateno, S., K. Hirose, Y. Ohishi, and Y. Tatsumi (2010), The structure of iron in Earth's inner core, *Science*, *330*, 359–361, doi:10.1126/science.1194662.
- Vinet, P., J. Ferrante, J. H. Rose, and J. R. Smith (1987), Compressibility of solids, *J. Geophys. Res.*, *92*, 9319–9325.
- Vočadlo, L., G. D. Price, and I. G. Wood (1999), Crystal structure, compressibility and possible phase transitions in  $\epsilon$ -FeSi studied by first-principles pseudopotential calculations, *Acta Crystallogr., Sect. B Struct. Sci.*, *55*, 484–493.
- Wade, J., and B. J. Wood (2005), Core formation and the oxidation state of the Earth, *Earth Planet. Sci. Lett.*, *236*, 78–95, doi:10.1016/j.epsl.2005.05.017.
- Zhang, F., and A. R. Oganov (2010), Iron silicides at pressures of the Earth's inner core, *Geophys. Res. Lett.*, *37*, L02305, doi:10.1029/2009GL041224.
- Zhang, J., and F. Guyot (1999a), Thermal equation of state of iron and  $\text{Fe}_{0.91}\text{Si}_{0.09}$ , *Phys. Chem. Minerals*, *26*, 206–211.
- Zhang, J., and F. Guyot (1999b), Experimental study of the bcc–fcc phase transformations in the Fe-rich system Fe–Si at high pressures, *Phys. Chem. Minerals*, *26*, 419–424.